Static and Cyclic Liquefaction of Copper Mine Tailings

Luis Vergaray[1]; Jorge Macedo, M.ASCE[2]; and Cody Arnold[3]

Abstract: Motivated by recent failures of tailings storage facilities (TSFs) around the globe, the tailings community is actively working to better understand the mechanical behavior of mine tailings. This study presents a geotechnical characterization (at both the laboratory and field scales) of copper mine tailings from a TSF located in an area with high seismicity, which makes assessing their response to static loading (e.g., static liquefaction) and earthquake-induced demands (e.g., cyclic-induced liquefaction) of primary importance. We discuss relevant aspects in the behavior of the examined mine tailings, including compressibility, stiffness, and the liquefaction (static and cyclic) response. Salient findings include the following: (1) the void index concept appears to characterize the compressibility of mine tailings regardless of ore source; (2) the stiffness-confinement dependence for the examined tailings contrasts with typical sand models; (3) theoretical particle size distributions that promote packing are useful for understanding trends in the location of the critical state line; (4) the examined tailings can experience static and cyclic liquefaction regardless of fine contents (insights on the observed responses are shared); (5) commonly used strain-based criteria are not robust enough to identify the cyclic liquefaction onset, thus we propose different criteria based on mechanistic descriptors; (6) the cyclic response of the examined tailings is affected by coupled stress-compressibility effects and their postliquefaction response fit within the expected response of natural silty soils; and (7) our assessment of state-of-practice liquefaction triggering procedures, in the context of the recently proposed ΔQ method, suggests a comparable performance for the tailings examined in this study. In addition, a soil behavior index (I_C) of 2.9 is consistent with the $\Delta Q = 20$ as suggested in the literature for assessing liquefaction susceptibility of the examined tailings. **DOI: 10.1061/JGGEFK.GTENG-10661.**

Introduction

The static liquefaction of mine tailings has caused numerous recent tailings storage facility (TSF) failures, such as the 2015 Fundao failure in Brazil, the 2018 Cadia failure in Australia, and the 2019 Brumadinho failure in Brazil. These failures have caused unprecedented devastating consequences for the environment, infrastructure damage, and loss of human life; they have been in the spotlight of the mining, engineering, and environmental communities (e.g., Morgenstern 2018; Jefferies 2022; Been 2016; Santamarina et al. 2019; Kossoff et al. 2014). For example, the 2015 Fundao and 2014 Mount Polley TSF failures are considered unprecedented environmental disasters in Brazil and Canada, respectively. In countries with moderate to significant seismicity and an active mining industry (e.g., Peru, Colombia, Chile, Argentina) or an emerging mining industry (e.g., Ecuador), the response of mine tailings to seismic loading is also of major concern. For instance, the magnitude 8.8, 2011 Maule earthquake in Chile caused the failure of the Las Palmas tailings dam, with evidence of seismic-induced liquefaction of the deposited tailings (GEER 2010). Recent worldwide TSF failures have triggered international debates regarding the safety of TSF systems and the mechanical response of mine tailings. In this context, Morgenstern (2018) evaluated contributory factors in 15 TSF incidents, classifying them into engineering, operations, and regulatory factors. Morgenstern's assessment highlighted that engineering (e.g., inadequate understanding of the mechanical response of mine tailings, inadequate site characterization, etc.) is one of the predominant contributory factors. Other experts (e.g., Jefferies 2022; Been 2016) reached conclusions similar to those of Morgenstern (2018), also highlighting the key role of understanding the response of mine tailings. Thus, advancing the geotechnics of mine tailings is crucial for the design and condition assessment of TSFs. This is particularly challenging as mine tailings are manmade geomaterials, generally classified as sandy silt to almost pure silt, and most approaches in geotechnical engineering have been developed for sands and clays; comparatively, very little exists on intermediate materials. Mine tailings are also geologically young materials, with angular grains rather than subrounded and often with lower proportions of quartz than many natural soils; thus, standard geotechnical correlations should not be taken as applicable to tailings without detailed consideration of these factors.

Previous efforts to study the mechanical response of mine tailings are somewhat limited when compared to natural soils (i.e., sands, clays) and have been mostly focused on the laboratory scale considering monotonic triaxial loading conditions (e.g., Jefferies and Been 2015; Shuttle and Jefferies 2016; Fourie and Tshabalala 2005; Carrera et al. 2011; Smith et al. 2019; Macedo and Vergaray 2021; Torres-Cruz and Santamarina 2019), and cyclic conditions using cyclic triaxial or cyclic simple shear tests (e.g., Wijewickreme et al. 2005a; James et al. 2011; Suazo et al. 2016; Geremew and Yanful 2013; Hu et al. 2017); however, it is rare to find studies that perform a comprehensive characterization of both the static and cyclic responses. In addition, only a few studies consider both laboratory and field-scale information to some extent (e.g., Shuttle and Jefferies 2016; Torres-Cruz 2016; Reid et al. 2018) and are typically focused on the response to static loadings. These previous studies emphasize that mine tailings have

[1]Graduate Student, School of Civil and Environmental Engineering, Georgia Institute of Technology, Atlanta, GA 30332. Email: luis.vergaray@gatech.edu

[2]Assistant Professor, School of Civil and Environmental Engineering, Georgia Institute of Technology, Atlanta, GA 30332 (corresponding author). ORCID: https://orcid.org/0000-0002-0457-4824. Email: jorge.macedo@gatech.edu

[3]Graduate Student, School of Civil and Environmental Engineering, Georgia Institute of Technology, Atlanta, GA 30332. Email: cody.arnold@gatech.edu

Note. This manuscript was submitted on December 23, 2021; approved on October 19, 2022; published online on February 28, 2023. Discussion period open until July 28, 2023; separate discussions must be submitted for individual papers. This paper is part of the ***Journal of Geotechnical and Geoenvironmental Engineering***, © ASCE, ISSN 1090-0241.

distinctive mechanical properties compared with what is commonly observed in natural soils, i.e., a higher frictional strength, higher dilatancy, and higher compressibility. These differences are attributed to the microstructure and mineralogy peculiar to mine tailings. Even though previous studies provide valuable insights, the tailings community is still actively working to better understand the mechanical behavior of mine tailings (e.g., Macedo et al. 2020), and part of this effort is directed toward increasing the number of case studies of the mechanical response of mine tailings. In particular, efforts that examine the response and properties of mine tailings at different scales (i.e., field and laboratory) considering static and cyclic loadings are desired, which is one of the contributions of this study.

This study presents a geotechnical characterization (at both the laboratory and field scales) of copper mine tailings from a TSF located in an area with high seismicity, which causes the assessment of their response to static loading (e.g., static liquefaction) and earthquake-induced demands (e.g., cyclic-induced liquefaction) to be of primary importance. In addition, the results from previous studies on mine tailings and natural soils are also integrated when deemed necessary with the goal of improving the overall understanding of the mechanical response of mine tailings. This study is structured as follows. After a general introduction, an overview is provided of the geotechnical field and laboratory program for characterizing the examined mine tailings in this study. We then discuss the compressibility and stiffness of the examined mine tailings. Next, we discuss aspects relevant to the triggering of static liquefaction, including the critical state line (CSL) dependence on particle properties and the proportion of particle sizes. Then we present the cyclic response of the examined mine tailings, sharing salient insights. Followed by a discussion on the assessment of earthquake induced liquefaction at a field scale. Finally, we close this study by presenting our conclusions.

Overview of Geotechnical Characterization

The geotechnical characterization program included *in situ* field testing such as cone penetration tests with pore pressure measurements (CPTu), shear wave velocity measurements using multichannel analysis of surface waves (MASW), and boreholes from which samples were recovered. Laboratory tests complemented the field testing by evaluating the monotonic and cyclic responses of the examined tailings considering three different gradations (denominated as S1, S2, and S3), which represent the range of deposited tailings (see details in Table 1). The laboratory program included oedometer tests, isotropic consolidation tests, triaxial compression tests, bender element tests, and cyclic simple shear (CSS) tests, with relevant details discussed later in the paper. Of note, the interpretations of our results often rely on the critical state soil mechanics (CSSM) framework applied to mine tailings. Due to space limitations, we cannot discuss the CSSM framework in detail, but interested readers are referred to Jefferies and Been (2016), who discuss the framework in the context of mine tailings.

Fig. 1 shows the different field tests conducted within the TSF schematically. The CPTu and MASW tests were performed in the tailings beach close to the dam, with three CPTu conducted in the west area, three CPTu in the central area, and four CPTu in the east area. In addition, geophysical tests were conducted in the tailings beach, which consisted of seven MASW lines. Fig. 2 shows the range of CPTu measurements (i.e., corrected tip resistance $-q_t$; friction resistance $-f_s$; pore pressures $-u_2$) for the different sections of the tailings beach. In addition, Fig. 2 shows the location of the CPTu data on the soil behavior type (SBTn) chart proposed by Robertson (2016), where SBTn is estimated from the normalized

Table 1. Index properties of the three representative gradations S1, S2, and S3

Material	Copper tailing S1	Copper tailing S2	Copper tailing S3
Plasticity index (PI)	NP	NP	NP
Fine content (FC)	15	38	75
Specific gravity (G_s)	2.70	2.60	2.75
Maximum void ratio (e_{max})	NA	1.00	1.13
Minimum void ratio (e_{min})	NA	0.541	0.604
Mean particle size (D_{50})	0.21	0.12	0.05
Coefficient of uniformity (C_u)	4.49	11.47	13.90

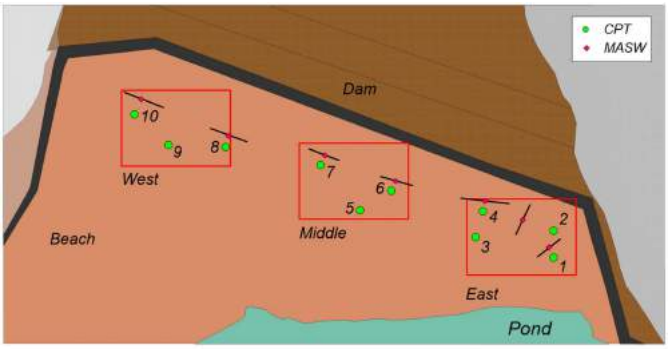

Fig. 1. TSF illustration, showing the location of field tests schematically.

cone resistance ($Q_{tn} = [q_t - \sigma_v/P_a](P_a/\sigma'_v)^n$) and the normalized friction ratio ($F_r = [f_s/(q_t - \sigma_v)] \times 100\%$), where σ_v and σ'_v are the *in situ* total and effective vertical stresses, respectively, and $n = 0.381I_c + 0.05(\sigma'_v/P_a) - 0.15$ is the stress exponent that depends on the soil behavior index (I_c) and atmospheric pressure (P_a). The tailings discharge deposition created a beach along the dam with a general profile composed of sandy silts and silty sands. There are, however, thin layers of finer materials. In general, the upper 15 m of material show q_t less than 5 MPa and a contractive response according to the SBTn plot; the deeper materials present a higher q_t with values up to 20 MPa.

Several samples were also recovered from boreholes, which were used to characterize index properties and perform laboratory tests. In this context, representative gradations for advanced laboratory testing were prepared according to the particle size distribution of samples recovered from the field. The index and particle distribution properties for the three representative gradations are summarized in Table 1. Various laboratory tests were conducted to evaluate the static and cyclic response of the S1, S2, and S3 gradations. In the following sections, we discuss these tests and highlight key observations that can shed light on the mechanical behavior of mine tailings.

Compressibility and Stiffness

Oedometer and isotropic consolidation tests were performed using the ASTM D2435-D2435M and ASTM D4767 procedures, respectively. A settled density was obtained for each gradation (S1, S2, and S3) from settling tests. Each gradation was then mixed to form a slurry at the desired settled density and then poured into an oedometer cell. For isotropic consolidation, once the slurry was prepared, it was poured into a membrane within a mold, and the specimen was frozen to preserve its shape. Then, the mold was

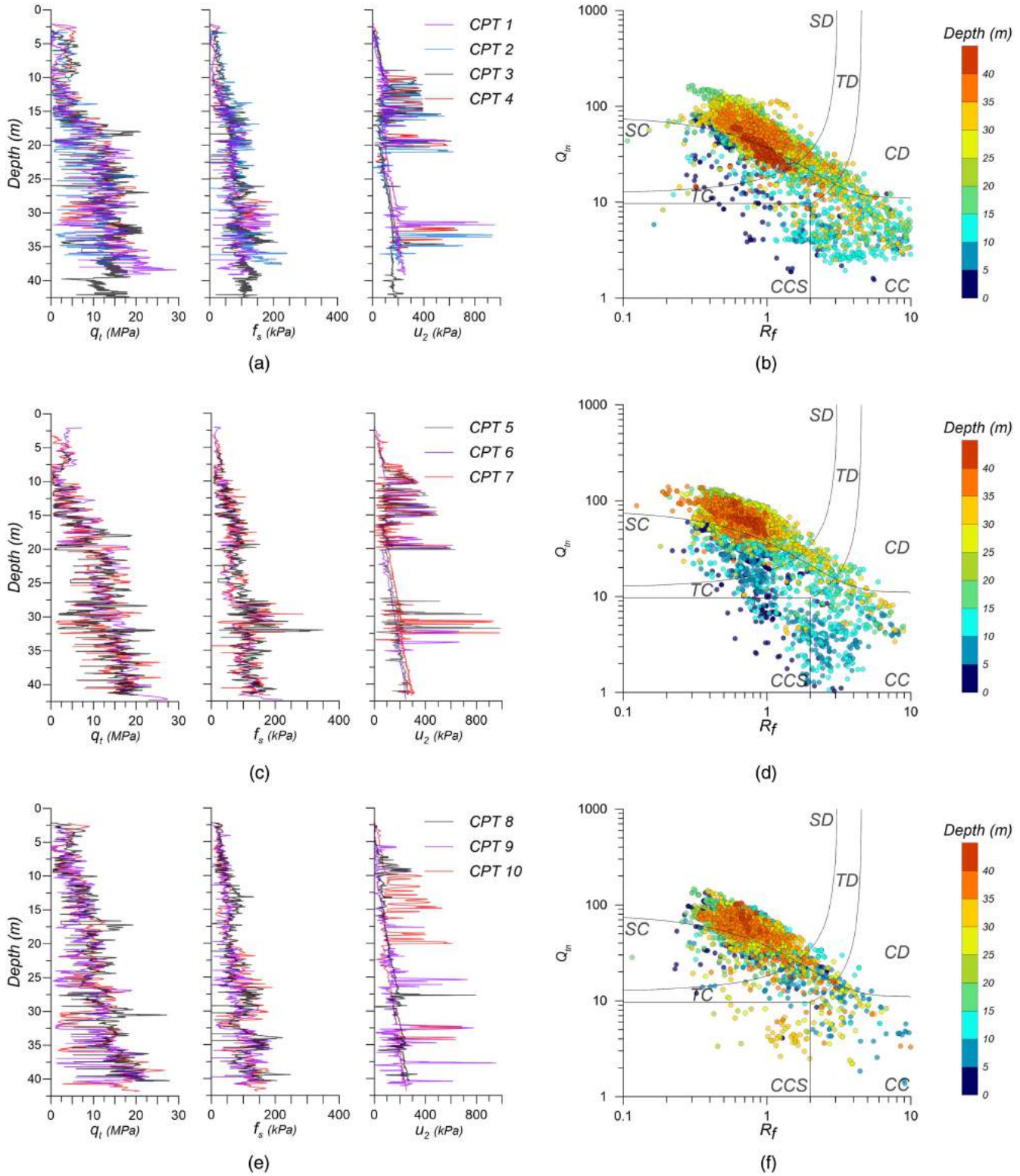

Fig. 2. q_t, f_s, and u_2 for CPT in the (a) east; (c) middle; and (e) west TSF areas. STBn (Robertson 2016) charts for the (b) east; (d) middle; and (f) west TSF areas. The SBTn zones are SC = sand-like contractive; SD = sand-like dilative; TC = transitional-like contractive; TD = transitional-like dilative; CC = clay-like contractive; CD = clay-like dilative; and CCS = clay-like contractive sensitive.

removed, and the frozen sample was placed inside a triaxial apparatus and allowed to thaw. Subsequently, back pressure is applied until saturation, and isotropic consolidation is conducted in stages until the targeted mean effective stress (p) is reached. Figs. 3(a–c) show the oedometer and isotropic consolidation tests results for the S1, S2, and S3 gradations. The consolidation behavior can be divided into three stages, as described by Wong et al. (2008) and presented in Fig. 3, considering the isotropic consolidation tests: (1) in the initial stage, the coarse sand grains are suspended in a matrix of fines at effective stresses (σ') lower than 1 kPa; (2) for

J. Geotech. Geoenviron. Eng., 2023, 149(5): 04023021

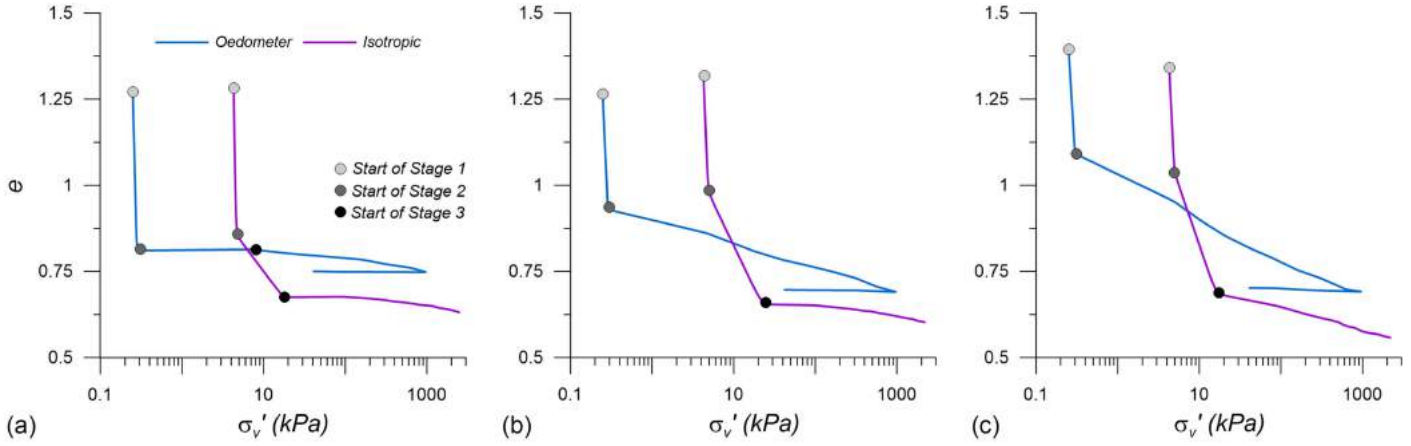

Fig. 3. Oedometer and isotropic consolidation tests for gradations: (a) S1; (b) S2; and (c) S3. The y axis in each figure indicates the void ratio (e) and the x axis the vertical effective stress (σ_v').

σ' values on the order of 20 kPa, the particles start to develop local contacts transmitting their self-weight; and (3) particles have developed a structure, and loads (e.g., self-weight imposed loads) can be transmitted through the soil skeleton. During the first stage, the samples are highly compressible, which is consistent with the self-weight consolidation process at low stresses described by Been and Sills (1981). Stage 2 shows a marked reduction in compressibility, which is followed by an additional decrease in stage 3. Of note, in the case of the oedometer tests, it is difficult to distinguish between stages 2 and 3 as the FC increases (i.e., gradations S2 and S3). This may be associated with the sparser tracking of points in the oedometer test compared to the isotropic consolidation test. Stages 1 to 3 also represent the expected consolidation process of deposited mine tailings, which are deposited as a slurry undergoing a self-weight consolidation (i.e., stage 1) before transmitting loads through the soil skeleton (i.e., stages 2 and 3).

The consolidation tests show that material S1 has lower compressibility than materials S2 and S3. In fact, the values of the compression index (Cc) for the S1, S2, and S3 specimens are 0.03, 0.07, and 0.09 from the oedometer tests, respectively. Another important aspect to consider from the consolidation lines is that even though the same reconstitution procedure (i.e., slurry deposition) was used, the consolidation lines are sensitive to the state of stresses (i.e., the anisotropy in the oedometer tests versus the isotropic conditions in the isotropic consolidation), with consistently lower void ratios achieved in the isotropic tests. To better compare the results from the oedometer and isotropic consolidation tests, we use the void index (I_v) introduced by Burland (1990) $I_v = \frac{e-e_{100}}{Cc}$ (where e_{100} is the void ratio at 100 kPa), which has also been applied to mine tailings in a few previous studies (Crowder 2004; Saebimoghaddam 2010; Suazo et al. 2016). Figs. 4(a–c) show the consolidation lines in the I_v versus σ_v' space for the gradations S1, S2, and S3. Interestingly, the I_v–σ_v' relationship is consistent for stresses larger than approximately 25 kPa for both the oedometer and isotropic consolidation tests, suggesting that the concept of an intrinsic consolidation line defined by Burland (1990) can be applied to the copper mine tailings examined in this study. Moreover, Fig. 4 also shows the I_v–σ_v' relationship for gold, silver, lead, and zinc tailings from Crowder (2004), Saebimoghaddam (2010), and Suazo et al. (2016). It can be noticed that the I_v–σ_v' relationship from these previous studies is consistent between them and is also consistent with the I_v–σ_v' relationship estimated in this study for copper tailings. This suggests that the I_v–σ_v' curves for mine tailings are in a narrow range regardless of ore type, which is an interesting feature that may be useful for constitutive modeling purposes, as it enables the normalization of consolidation curves. The applicability of the I_v concept to mine tailings highlights their significant compressibility (i.e., their change in density is significantly affected by changes in stresses), which is expected to affect their initial state and, hence, their static and cyclic resistance.

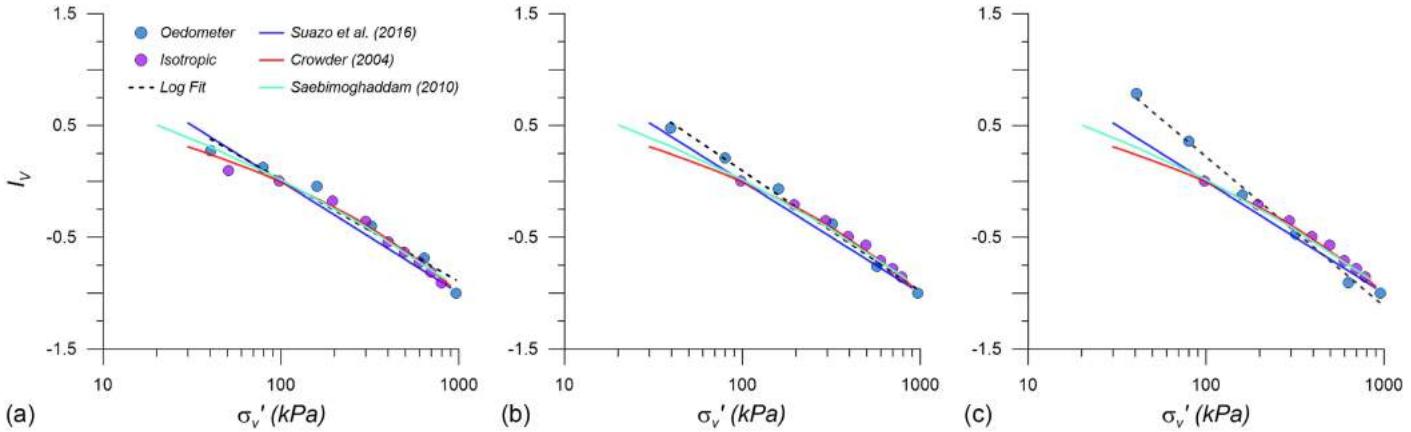

Fig. 4. I_v versus σ_v' curves for gradations: (a) S1; (b) S2; and (c) S3. (Data from Crowder 2004; Saebimoghaddam 2010; Suazo et al. 2016.)

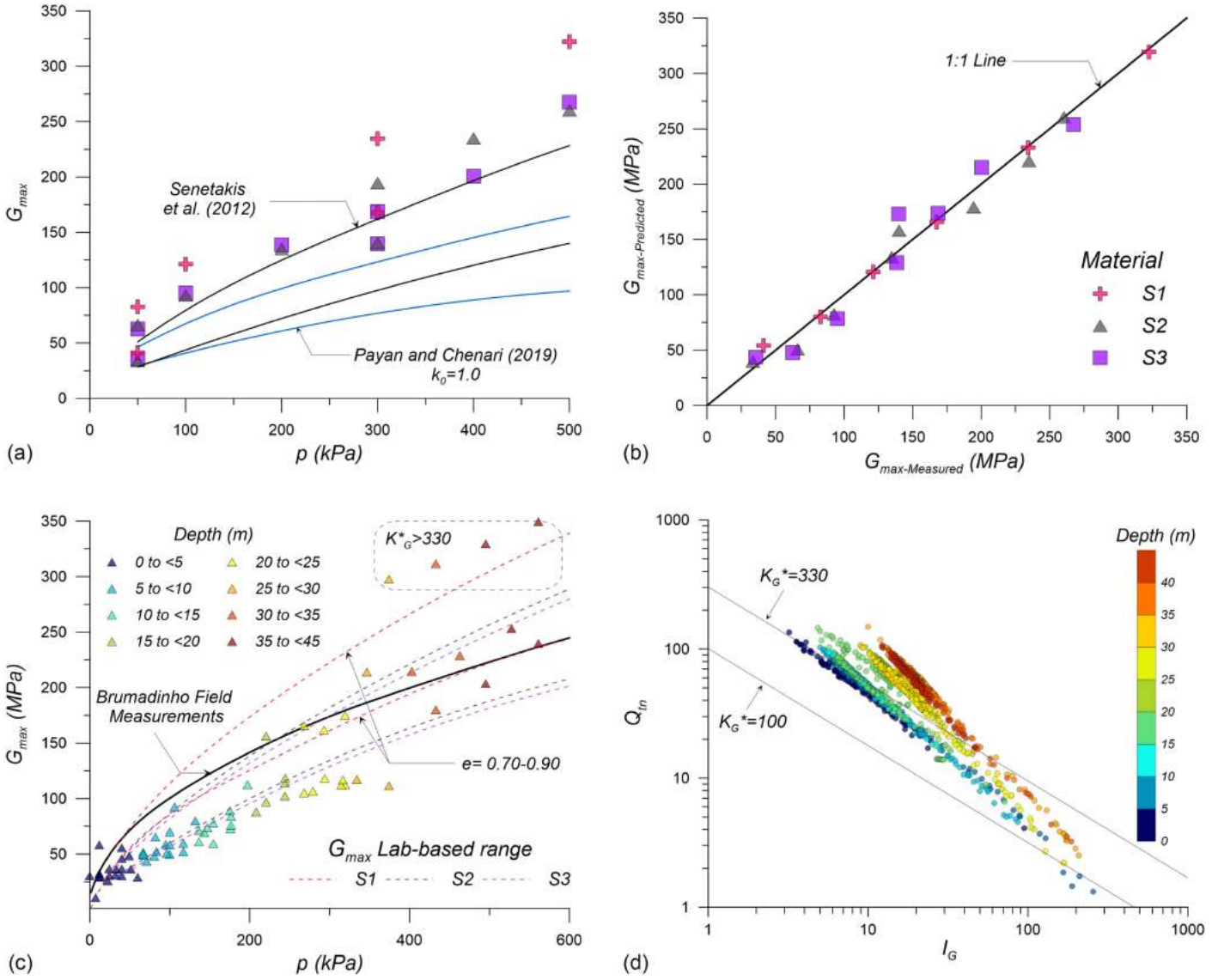

Fig. 5. (a) $G_{\max}$ for gradations S1, S2, and S3, along with estimates from $G_{\max}$ models for sands; (b) comparison of predicted versus measured $G_{\max}$; (c) $G_{\max}$ comparison for laboratory (dashed lines) and field scales (triangles); and (d) Q_{tn} versus I_G for selected CPTs.

Fig. 5 illustrates the elastic shear modulus ($G_{\max}$) estimated through bender element tests in the laboratory [Fig. 5(a)] and MASW tests in the field [Fig. 5(c)]. $G_{\max}$ was calculated from the shear wave velocity (V_s) values considering the relation $G_{\max} = V_s^2\rho$, where ρ is the soil density. ρ was measured in the laboratory tests and estimated from the water content (W) and specific gravity (G_s) in the field tests. Fig. 5(a) also shows estimates from the Payan and Chenari (2019) and Senetakis et al. (2012) $G_{\max}$ models formulated for sands for comparison purposes. The Payan and Chenari (2019) $G_{\max}$ model uses C_u (taken as the value for S1), a shape factor (i.e., regularity r, taken as 0.5, which is representative of crushed materials such as mine tailings), the at-rest pressure coefficient (K_0, taken as 1 as the bender tests were performed under isotropic conditions), and the void ratio (considered as $e = 0.7 - 0.9$, representative of the observed range from the field). The Senetakis et al. (2012) model also depends on the type of sand; hence, we selected the model for quarry sands, as mine tailings are also a product of rock crushing. Under these considerations, it can be observed that the trends from the referred models depart from the mine tailings results in most cases. In addition, note that the $G_{\max}$ values for the S1 gradation are higher than the values observed in the S2 and S3 gradations, which in turn are more similar. This observation is consistent with the findings in Payan et al. (2016) and Goudarzy et al. (2016), who stated that $G_{\max}$ for sand mixtures decreases with increasing FC up to 20%–35%, after which $G_{\max}$ does not change significantly even if FC continues to increase. Given the discrepancies between the referred models and the examined tailings, we used our data and the functional form in Payan and Chenari (2019) to derive a $G_{\max}$ model for the mine tailings investigated in this study. The derived model is $G_{\max} = 108 \times C_u^{-0.23} \times e^{-1.29\left(\frac{p}{P_a}\right)^{0.56C_u^{0.04}}}$, and its predictions are compared against the experimental data in Fig. 5(b), showing good performance (the 1:1 line indicates the case in which the prediction and experimental values are the same). The robustness of this equation for other mine tailings should be explored in future studies. We use this relationship to compare the laboratory-based $G_{\max}$ estimations (considering upper and lower estimates based on the range of observed e values) against the field estimations, as shown in Fig. 5(c). In estimating p for field conditions, K_0, is needed. We considered a value of 0.5, which is often used in deposited mine tailings (e.g., Jefferies and Been 2015).

J. Geotech. Geoenviron. Eng., 2023, 149(5): 04023021

Fig. 5(c) also shows the G_{max} values from the Brumadinho case history (Robertson et al. 2019), which are comparable to our field-based G_{max} values. From Fig. 5(c), it can be observed that for the first 15 m, the laboratory-based G_{max} values are higher than the field values, which might be associated with potential fabric differences between the laboratory reconstituted specimens and the deposited tailings. The bender element tests were performed on specimens reconstituted using moist tamping (MT), which may not be a good representation of the fabric of deposited mine tailings (e.g., Daliri et al. 2015); nevertheless, it is becoming the preferred method for reconstituting mine tailings for triaxial testing where benders tests are often also performed, as in this study (see discussion in next section). The dependence of G_{max} on the reconstitution procedure used in the laboratory (i.e., fabric) has also been emphasized by De Alba et al. (1984), Rashidian et al. (1995), and Gu et al. (2015). For instance, Gu et al. (2015) noted that G_{max} measured on moist tamped specimens can be up to 21% higher than air-pluviated and dry tamped specimens for similar void ratios and mean confining pressures. Interestingly, for depths below 15 m, the field-based G_{max} is more comparable to the laboratory-based values and, in some cases, larger. To put this observation in context, we use the normalized small-strain rigidity index $K_G^* = I_G Q_{tn}^{0.75}$ proposed by Robertson (2016), where $I_G = G_{max}/(q_t - \sigma_v)$ is the small-strain rigidity index. For K_G^* values between 100 and 330, soils are expected to be young without important microstructure effects; in contrast, $K_G^* > 330$ suggests the presence of a significant microstructure (e.g., aging, bonding). Fig. 5(d) shows the $I_G - Q_{tn}$ values plotted to assess microstructure effects, using representative CPTs. It is interesting to see that for layers between 15 and 40 m, there are areas with $K_G^* > 330$, which may be potentially attributed to bonding effects that increase G_{max}. Similar observations on deposited mine tailings have also been noted by Robertson et al. (2019).

Response on Triaxial Shearing, Critical State Location, and Static Liquefaction

The response of the examined mine tailings to monotonic loading was examined based on 10, 9, and 9 triaxial (TX) compression tests under drained and undrained conditions for gradations S1, S2, and S3, respectively. The tests were conducted using the ASTM D4767 and ASTM D7181 procedures. As elaborated in this section, these tests are also used to assess the CSL and evaluate the conditions for static liquefaction. The moist tamping procedure was the preferred reconstitution method, with the end-of-test freezing being used for void ratio measurement. Specimens were prepared by mixing water to a moisture content of approximately 5% and allowing the specimens to cure at this moisture content. The specimens were then reconstituted in six layers of varying weight using the "undercompaction" method (Ladd 1978). Additional details on the moist tamping procedure and end-of-test freezing void ratio measurement can be found in Jefferies and Been (2016). Of note, this procedure is becoming the standard procedure in practice (e.g., Reid et al. 2020), as also reflected in the forensic studies after recent TSF failures (e.g., Morgenstern et al. 2019; Robertson et al. 2019). Lastly, some tests using the slurry deposition method (e.g., Chang et al. 2011) were also considered. In this case, the specimens were prepared as slurries, following the same procedures discussed before for isotropic consolidation tests.

Figs. 6(a–c) show the stress path for individual tests in the $e - p$ space and the interpretations for the CSL for gradations S1, S2, and S3, considering linear and curved CSLs. Of note, the specimens prepared using slurry deposition (red lines) tend toward the same CSL evaluated using the moist tamped specimens, which is consistent with the findings of Reid and Fanni (2020) and supports the idea of a unique CSL that is independent of the initial fabric. Figs. 6(a–c) also show the relative location of the CSL (showing both the curve and linear adjustment) and the oedometer consolidation lines. It can be observed that, as FC increases, these lines tend to be more parallel within the considered range of stresses. This tendency for parallelisms as the FC increases has also been pointed out by Olson and Stark (2003) when examining the response of silty sands. Moreover, the slope of the CSL line does not change significantly as the FC increases, which is also consistent with the findings of Olson and Stark (2003) for natural soils, who pointed out that general trends between the CSL's slope and FC cannot be established. This suggests that FC is not a solid proxy for compressibility, as is often considered in state-of-practice liquefaction procedures (e.g., Youd and Idriss 2001). Fig. 6(d) also shows that the CSLs tend to move downward in the $e - p$ space as FC increases. Different studies have contrasting findings in terms of the influence of FC on the CSL location. For example, Carrera et al. (2011), examining the Stava tailings, found that the relative location of the CSL was controlled by a "transitional FC" (FC_{th}, equal to 50% in their study) below which the CSL moved downward (in the e versus p space) with increasing FC and above which the CSLs moved upward. Of note, FC_{th} has been defined based on binary mixtures where the effects of adding fines on a host coarser matrix are evaluated (e.g., Lade and Yamamuro 1997; Thevanayagam et al. 2002; Thevanayagam 2007; Carrera et al. 2011). In other efforts, such as the study by Li and Coop (2019), which focused on iron tailings, the CSL showed only an upward transition as FC increased. In contrast, our results show only a downward transition. We are only aware of the study by Fourie and Papageorgiou (2001), which showed a similar pattern, but their study was limited to an FC of 60%. Our results and previous studies considering natural gradations suggest that the FC_{th} concept (formulated using artificial gradations) might not be appropriate for mine tailings, which often have a broad range of particles. Moreover, FC alone is not a robust descriptor for the trends in the CSL movement.

Interpretation of CSL Location in Terms of Particle Properties and Packing Indices

In a broader sense, the altitude and slope of a CSL (i.e., its position) are affected by the overall particle size distribution (e.g., Poulos et al. 1985; Wood and Maeda 2007; Yan and Dong 2011; Li et al. 2014; Yang and Luo 2017), particle properties (e.g., roundness) as shown by Poulos et al. (1985) and Cho et al. (2006), and mineralogy. To illustrate this, Fig. 7(a) uses data from this study; 53 additional mine tailings from Shuttle and Cunning (2007), Anderson and Eldridge (2011), Bedin et al. (2012), Schnaid et al. (2013), Been (2016), Li et al. (2018), Li and Coop (2019), Raposo (2016), Torres-Cruz (2016), Morgenstern et al. (2016), Riemer et al. (2017), Li (2017), Robertson et al. (2019), Macedo and Petalas (2019), Gill (2019), Reid and Fanni (2020), Reid et al. (2018, 2020), Fourie and Papageorgiou (2001), and Carrera et al. (2011); sands from Cho et al. (2006); and data from Houston sand (HS), glass beads (GB), and DEM simulations from Li et al. (2014). This figure illustrates how the influence of particle properties and grading (using C_u as a proxy) affects the altitude of the CSL. We use Γ_{100} (i.e., the altitude of the CSL at 100 kPa) as it is often better defined than Γ (the altitude at 1 kPa) as discussed in Torres-Cruz and Santamarina (2019). The highlighted data in Fig. 7 are from the Cho et al. (2006) study, where C_u was purposely constrained to a small range to distill the effects of particle shape. Note how Γ_{100} decreases as the roundness increases, and that the Γ_{100} values for particles with lower roundness are within the range observed for

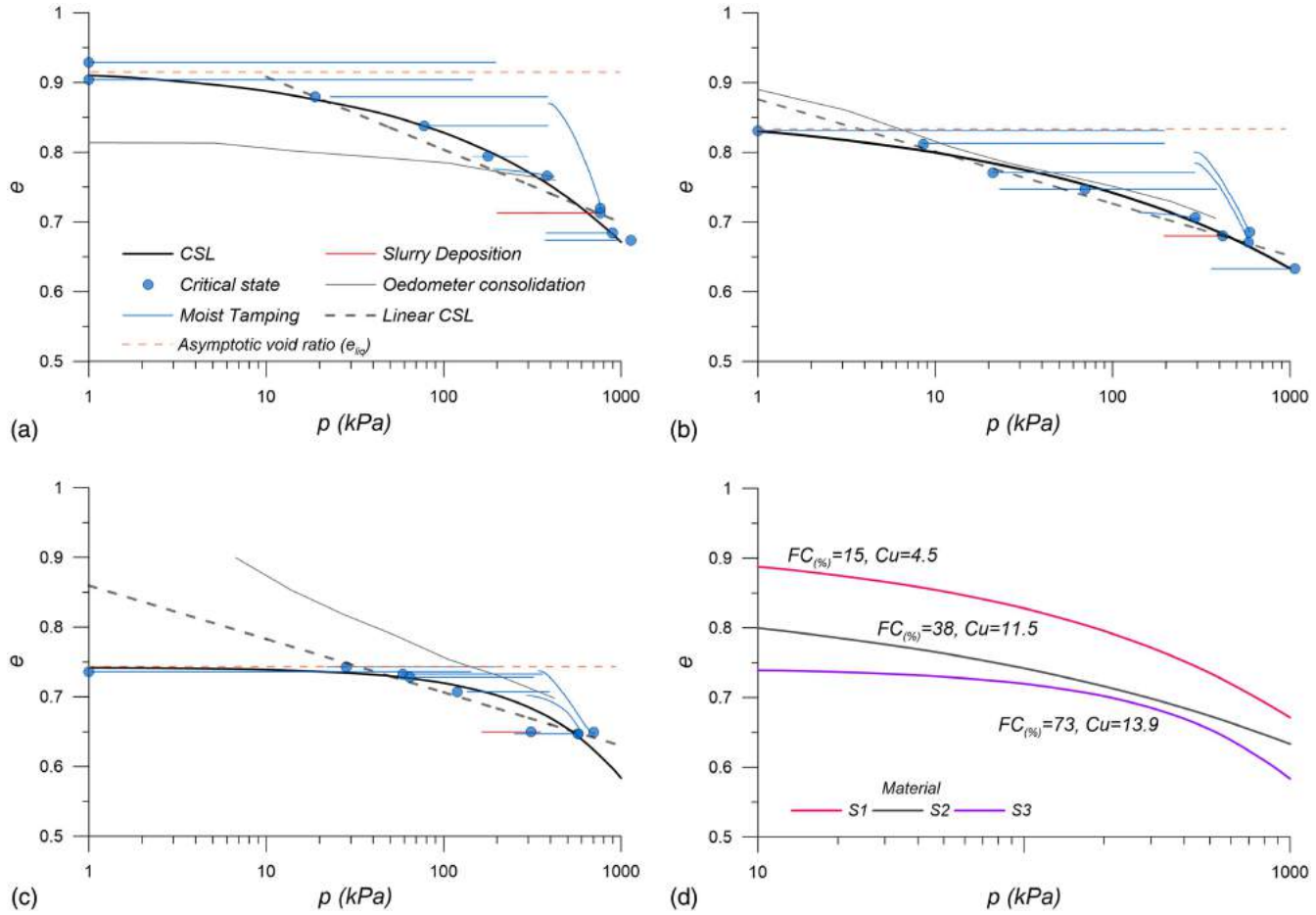

Fig. 6. Triaxial test results in the $e - p$ space, along with linear and curve CSL idealizations for gradations: (a) S1; (b) S2; (c) S3; and (d) CSLs for gradations S1, S2, and S3.

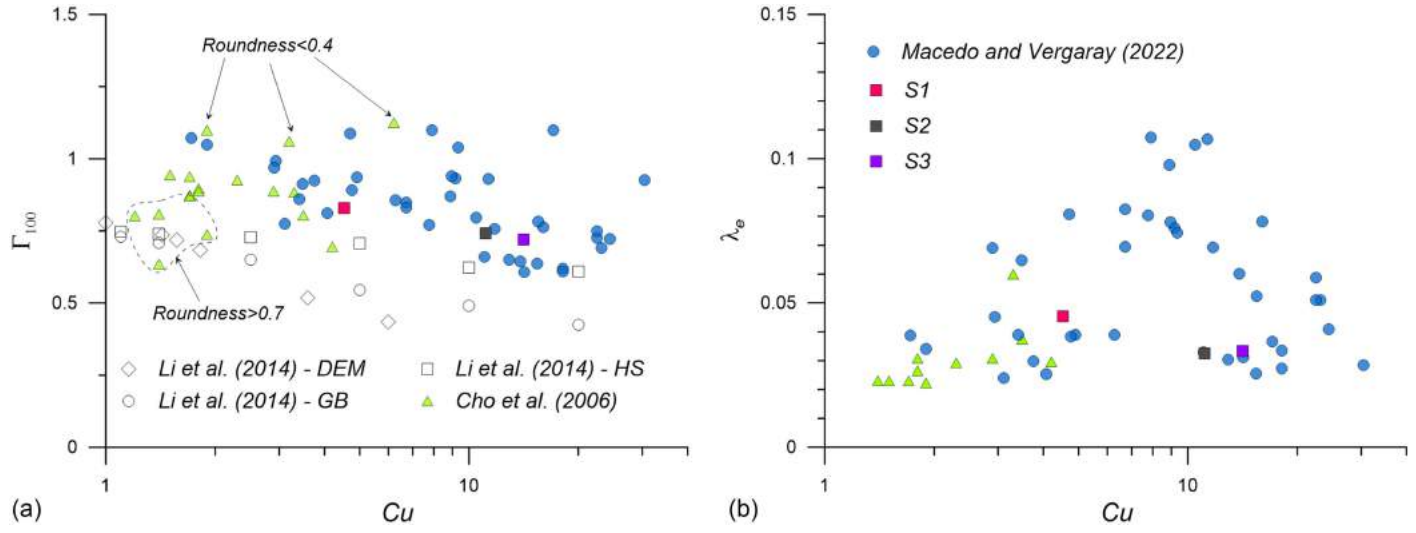

Fig. 7. (a) Comparison of Γ_{100} versus C_u; and (b) λ_e versus C_u for sands (Cho et al. 2006; Li et al. 2014) and mine tailings (see the text for details). HS = Houston Sands; GB = glass beds; and DEM = discrete element modeling.

mine tailings, which typically have a low roundness due to the processes involved in their generation. Note also how the Γ_{100} from glass beads and DEM simulations (with spherical particles) are consistent with the Γ_{100} for sands with high roundness and lower than Γ_{100} for mine tailings, indicating the role of particle shape. Fig. 7(b) shows the CSL slope (λ_e) variation in terms of C_u considering the mine tailings from this study and the mine tailings from past studies previously described. It is interesting to see how λ_e

tends to increase with C_u up to values on the order of 7–8 and then decreases as C_u keeps increasing. These trends can be interpreted considering the theoretical particle size distributions derived by Lade et al. (1998) that promote enhanced packing (i.e., a low e). Lade et al. (1998) used results from McGeary (1961) and found that the $e_{\min}$ for binary packing of particles will decrease rapidly as the ratio of coarse and fine particle sizes (D/d) increases up to 7, after which $e_{\min}$ keeps decreasing, but at a lower rate; hence, they stated that $D/d = 7$ efficiently creates an enhanced packing. Using this result, Lade et al. (1998) proposed a range for theoretical particle size distribution curves, presented in Fig. 8 along with an experimental-based range from McGeary (1961). Lade et al. (1998) also defined a "smooth grain size distribution" curve, corresponding to the trend line through the midpoints of the vertical lines (Fig. 8). Fig. 8 also presents the normalized particle size distributions for the mine tailings in Fig. 7. The particle sizes were normalized by the size at which 75% of particles are finer and then scaled by a factor of 343 for direct comparison against the theoretical-based curves from Lade et al. (1998). Interestingly, the particle size distributions of the materials with a $C_u > 8$ are generally consistent with the theoretical ranges from Lade et al. (1998), indicating that these gradations promote an enhanced packing (i.e., a lower CSL slope) as the difference in particle sizes increases, i.e., as C_u increases, using C_u as a proxy for particle sizes. On the other hand, the gradations for the materials with $C_u < 8$ are generally not consistent with the theoretical ranges proposed by Lade et al. (1998); hence, they do not favor enhanced packing as the proportion of particle sizes increases (i.e., as C_u increases). Instead, the trend suggests that fine particles may contribute to separating coarser particles, creating looser packing (i.e., a higher CSL slope), which was also suggested by Lade et al. (1998) when the proportion of particle sizes is small (i.e., a low C_u). It is important to emphasize that C_u is used only as a proxy for the proportion of particle sizes, and it is not expected that C_u will capture details of the full particle size distribution or particle-based properties, which is consistent with the significant scatter observed in Figs. 7(a and b).

Static Liquefaction

Carrera et al. (2011) and Bedin et al. (2012) pointed out that a curved CSL gives rise to a changing susceptibility to liquefaction as the stress level increases. When the soil's initial void ratio (e_0) lies above the horizontal asymptote of the CSL in the $e - p$ plane [denoted as e_{liq} in Figs. 9(a) and Fig. 6], full static liquefaction occurs [i.e., deviatoric stress (q) tends to zero; see representative examples for our materials in Fig. 9(b)] under undrained loading because the critical state is "undefined" in the $e - p$ plane (see the stress paths above e_{liq} in Fig. 6). With increased confining pressure, e_0 will lie below the horizontal asymptote, leading to a strain-softening response where the final q is not zero, which was defined as partial softening by Macedo and Vergaray (2021) and Soares and Fonseca (2016). This response is also often referred to as flow failure or flow instability (e.g., Sladen et al. 1985; Chu and Leong 2002); see representative examples in Fig. 9(b). As p increases further and the CSL becomes steeper (Fig. 6), a limited flow behavior (i.e., showing a transition from contractive to dilative behavior after the peak) is observed, as illustrated in Fig. 9(b). It is worth highlighting that these responses, i.e., full static liquefaction, flow instability, and limited flow, have the potential to cause uncontrolled deformations, as observed in recent case histories (e.g., Robertson et al. 2019; Morgenstern et al. 2019). Finally, a nonflow response, associated with hardening behavior, occurs when e_0 lies below the CSL (Fig. 6). Li and Coop (2019) and Li et al. (2018) used the horizontal asymptote of curved CSLs in the $e - p$ plane (Fig. 6) to assess full static liquefaction susceptibility for iron and gold tailings. Our assessment of the copper mine tailings examined in this study is presented in Fig. 9(a). Consistent with Li and Coop (2019), the vertical bars in Fig. 9(a) are based on the range of void ratios observed on consolidation tests, and maximum/minimum void ratios measured through ASTM procedures (i.e., $e_{\min-ASTM}$, $e_{\max-ASTM}$) are also included, but only referentially since these testing procedures are strictly applicable only to sands with small fine contents. Fig. 9(a) also shows the range (vertical bars) of void ratios for mine tailings in previous studies (i.e., Li and Coop 2019; Li et al. 2018; Li 2017; Carrera et al. 2011), their associated e_{liq} values (markers on each bar), and the upper and lower void ratio ranges suggested by Li et al. (2018). These ranges are generally consistent with the ranges observed in this study. An interesting observation is that the three gradations (S1, S2, and S3) can develop full static liquefaction, as can be noticed from e_0 in Fig. 6 that are above e_{liq} and the stress–strain responses in Fig. 9(b), which also illustrate how the

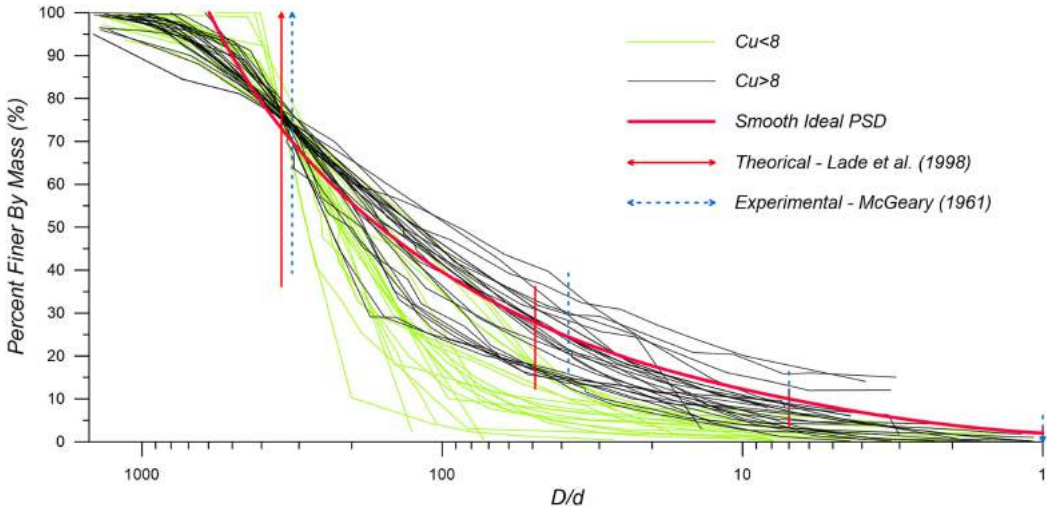

Fig. 8. Particle size distributions to produce optimal quaternary packing of spherical particles from Lade et al. (1998) and McGeary (1961) along with the normalized particle size distributions of several tailings (see the text for details).

J. Geotech. Geoenviron. Eng., 2023, 149(5): 04023021

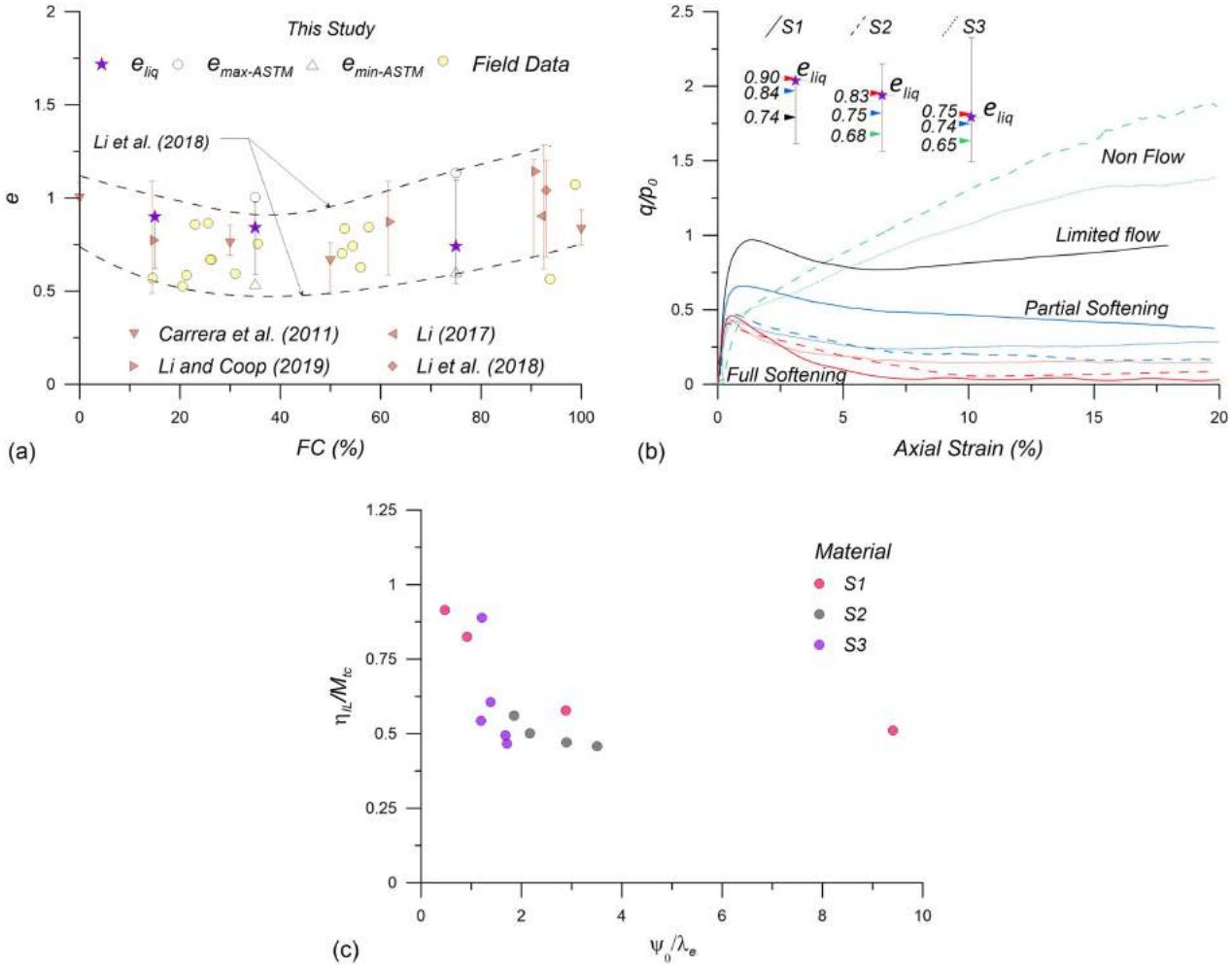

Fig. 9. (a) Range of void ratios in the laboratory and the field for gradations S1, S2, and S3 along with data from previous studies. The vertical bar indicates the range of void ratios observed in the laboratory, and e_{liq} is the horizontal asymptote to a curve CSL (see Fig. 7); other terms are defined in the text. (b) Illustration of the transition from full static liquefaction, partial softening, limited flow, and nonflow behavior for materials examined in this study. (c) $\frac{\eta_{IL}}{M_{tc}}$ versus $\frac{\psi_0}{\lambda_e}$ for gradations S1, S2, and S3.

behavior transitions from full static liquefaction to partial softening and limited flow as e_0 becomes lower than e_{liq} but stays above the CSL. The observation of full static liquefaction for gradation S3 with the largest FC is in contrast with Li and Coop (2019), who did not observe full static liquefaction for the iron tailings they examined when the FC was large (i.e., 90%). Other studies have shown a larger liquefaction potential as FC increases (e.g., Carrera et al. 2011, who examined the Stava tailings). Thus, relying on FC to assess the expected response of mine tailings, such as the triggering of static liquefaction, is misleading. Instead, engineers should rely on mechanistic-based parameters that are intended to represent the effects of the mineralogy and particle properties in the mechanical response of mine tailings.

Fig. 9(c) shows the dependence of the normalized stress ratio at the peak of the stress path ($\frac{\eta_{IL}}{M_{tc}}$) with respect to the normalized state parameter ($\frac{\psi_0}{\lambda_e}$), considering the three gradations S1, S2, and S3. Normalized parameters are used consistently with Macedo and Vergaray (2021) to provide compressibility and strength information. It can be noticed that ($\frac{\eta_{IL}}{M_{tc}}$) decreases as $\frac{\psi_0}{\lambda_e}$ increases, which is consistent with Macedo and Vergaray (2021) and Yang (2002), emphasizing the dependence of the instability triggering on the state of tailings.

Going back to the discussion on mechanistic-based parameters, under the CSSM framework, the parameters are (1) CSL-based, i.e., Γ, λ_e if the CSL is defined as $e_{cs} = \Gamma - \lambda_e \ln(p)$ or a, b, and c for a curved CSL defined as $e_{cs} = a - b(p/P_a)^c$, where e_{cs} is the void ratio at the critical state; (2) stress dilatancy-based, such as M_{tc} (the critical state stress ratio) and N (volumetric coupling), which are related through $\eta_{\max} = M_{tc} + (1 - D_{\min})N$, where $\eta_{\max}$ is the maximum stress ratio and $D_{\min}$ is the maximum dilatancy; (3) state dilatancy-based, i.e., χ, which relates the maximum dilatancy with the state through $D_{\min} = \chi\psi$, where ψ is the state parameter defined by Been and Jefferies (1985); and (4) stiffness-based, such as (G_0), which scales the dependence of $G_{\max}$ in terms of p, i.e., $G_{\max} = G_0 \cdot (p/P_a)^B$. It is important to note that Γ, λ_e, M_{tc}, N, χ, and $G_{\max}$ are often present as parameters in robust constitutive models, usually formulated for sands (although often named differently or represented by other proxies), and are the basis for the current mechanical-based understanding of static liquefaction (e.g., Jefferies and Been 2015), as also reflected by their use in forensic studies of recent TSF failures (e.g., Morgenstern et al. 2016, 2019; Robertson et al. 2019). One of these models is Norsand (Jefferies 1993), which is selected in this study to illustrate how a range of responses from static liquefaction to hardening for the

three gradations S1, S2, and S3 can be reasonably reproduced using the same set of parameters. Norsand is selected because of its simplicity as it uses all of the mechanistic-based parameters previously discussed and only requires an additional parameter (the plastic modulus, H) that can be assessed during calibrations. Γ, λ_e (or a, b, and c) can be estimated from Fig. 6; M_{tc} can be estimated as the ratio of q and p at the critical state, and the estimation of $G_{\max}$ is based on bender element tests (i.e., Fig. 5). Finally due to the limited number of drained tests, N, χ, and H were estimated through forward-inverse modeling with Norsand (Jefferies 1993). The Appendix shows the final set of calibrated parameters. Fig. 10 shows examples of Norsand simulations considering the three gradations S1, S2, and S3 along with static liquefaction and hardening responses, showing consistency between the experiments and simulations. Hence, once the mechanical parameters (Γ, λ_e, M_{tc}, N, χ, and $G_{\max}$) are assessed, different ranges of responses can be estimated, and static liquefaction becomes just another manifestation of the behavior of a particulate medium. Norsand is just one of the existing CSSM-based models; other models include, for example, the Sanisand family (e.g., Dafalias and Manzari 2004; Li and Dafalias 2012; Petalas et al. 2018).

Cyclic Response

The cyclic response for the three gradations S1, S2, and S3 previously described was assessed based on CSS testing. These tests considered specimens of 70 mm in diameter and height of approximately 25 mm (after consolidation), which were contained within a series of Teflon-coated, low-friction rings that restrain lateral deformation. The tailings were prepared as a slurry following procedures similar to those previously discussed and spooned inside the CSS rings, which were lined with a latex membrane, before placing the top platen. The specimen was secured with an O-ring on the top platen and was allowed to consolidate in stages to the desired vertical effective stress. After consolidation, the tailings were subjected to cyclic loading by applying sinusoidal shear stress of constant amplitude, keeping the volume constant to simulate undrained conditions. After the cyclic loading phase, each specimen was reconsolidated to the initial vertical effective stress to obtain the postcyclic volumetric strain through postcyclic reconsolidation. Fig. 11 presents representative results for the three mine tailings gradations considering a cyclic stress ratio ($CSR = \tau/\sigma'_{v0}$, where τ represents the targeted maximum shear stress during cyclic loading and σ'_{v0} is the initial vertical effective stress) of 0.12, $\sigma'_{v0} =$ 300 kPa and similar initial states (i.e., $\psi_0 = 0.72 - 0.85$). The results for all CSS tests are presented in Figs. S1–S28.

Fig. 11 shows that the three gradations present stress–strain loops with a significant degradation in stiffness, the stress paths move to the left until stabilizing near vertical effective stresses close to 0, the excess pore pressure ratio [$R_u = (\sigma'_{v0} - \sigma'_v)/\sigma'_{v0}$] reaches values of 1 or near 1, and the shear strains start to accumulate rapidly after several cycles. Similar behaviors were also observed for

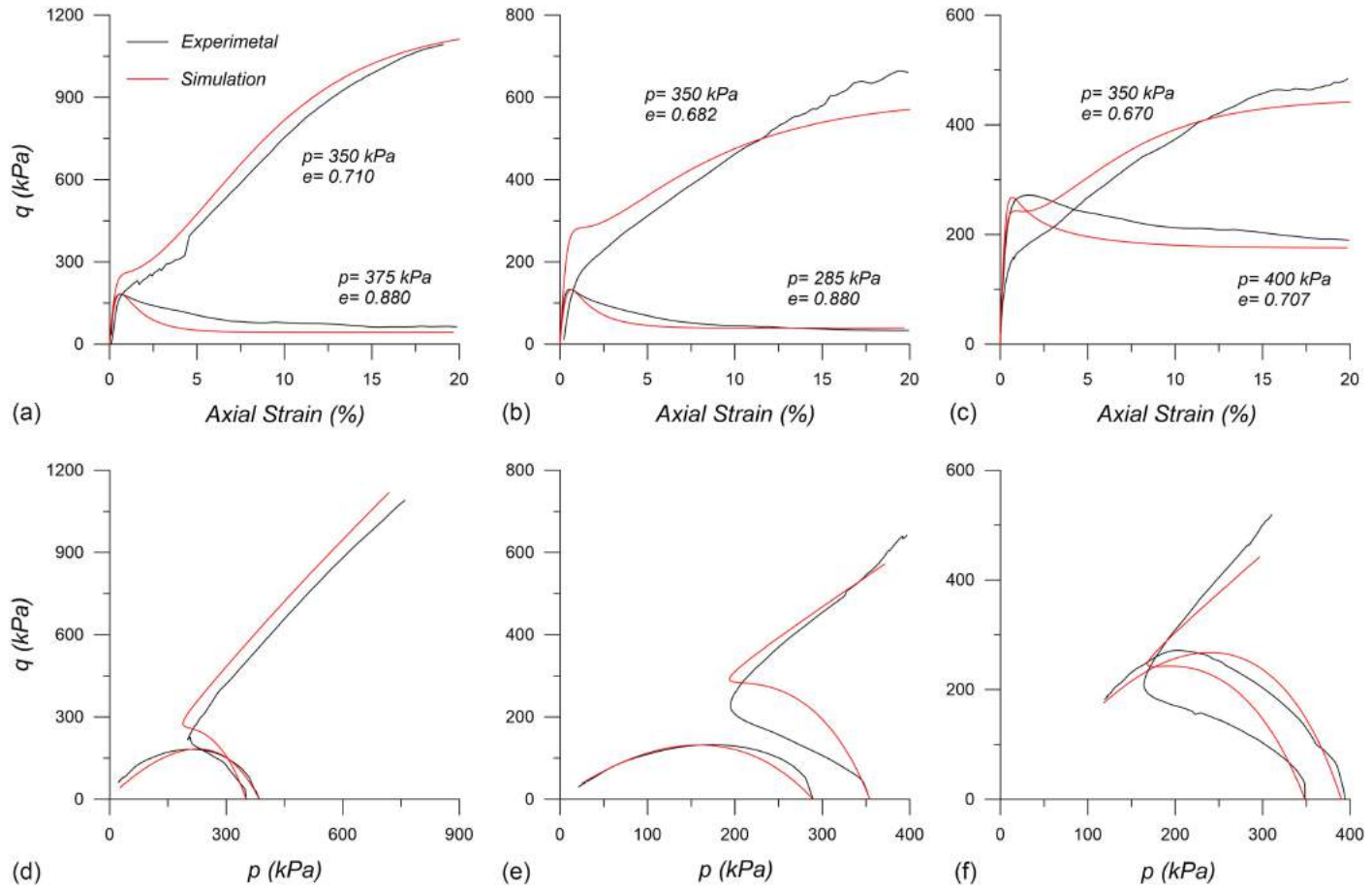

Fig. 10. Stress–strain response from experiments and simulations for gradations: (a) S1; (b) S2; and (c) S3. Stress paths for experiments and simulations for gradations: (d) S1; (e) S2; and (f) S3.

J. Geotech. Geoenviron. Eng., 2023, 149(5): 04023021

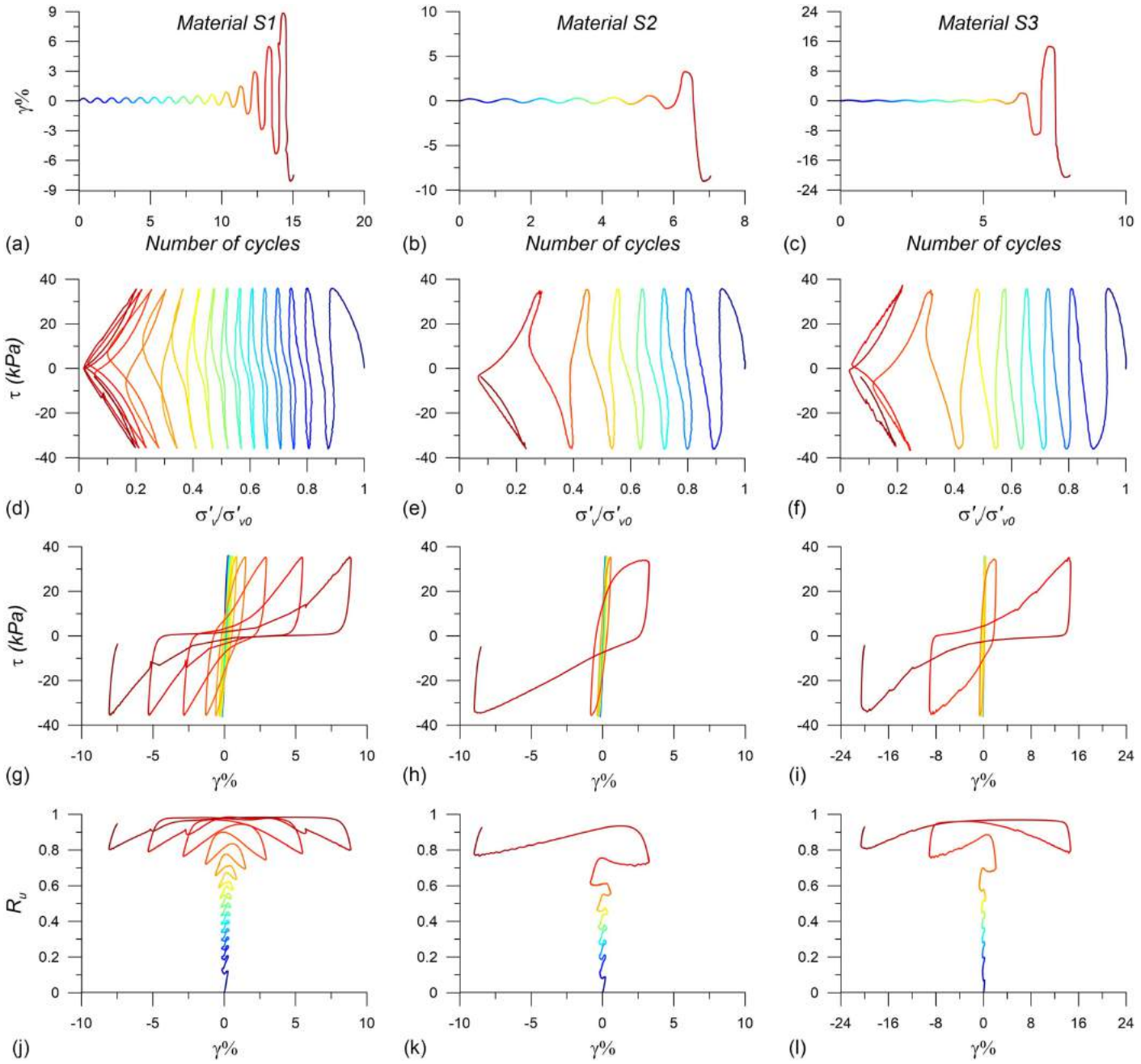

Fig. 11. CSS test for materials S1, S2, and S3 (from left to right) at $\sigma'_{v0} = 300$ kPa and $CSR = 0.12$: (a–c) number of cycles versus shear strain [γ (%)]; (d–f) σ'_v versus τ; (g–i) τ versus γ (%); and (j–l) γ (%) versus R_u.

other tests; i.e., the mine tailings liquefied with a large degradation of stiffness and generated large uncontrolled strains. The posttriggering behavior of increasing shear strain accumulation per cycle, seen in Fig. 13(a), contrasts with what has been noted for sands, which often see a constant accumulation of posttriggering shear strains (Tasiopoulou et al. 2020). Bray and Sancio (2006) proposed a criterion in terms of index properties (i.e., PI, liquid limit – LL, and W) to assess the expected cyclic response of fine-grained soils, which is presented in Fig. 12, along with the data for our mine tailings. According to the Bray and Sancio (2006) criterion, our tailings are located in the "susceptible to liquefaction" zone because $W/LL > 1$ and $PI < 12$, which is consistent with the observed response during cyclic loading. Wijewickreme et al. (2005a) also found that the Bray and Sancio (2006) criterion was adequate for the copper, gold, and zinc tailings they examined. Hence, these observations suggest that the Bray and Sancio (2006) criterion might be adequate for mine tailings and reinforce their observation that FC is not fundamental to assess the expected cyclic response in fine-grained soils. (As shown in Fig. 12, we observe liquefaction regardless of the FC.)

We now discuss typical cyclic responses for the mine tailings examined in this study; Fig. 13 shows the test results [Figs. 13(a–c)] and typical patterns [Figs. 13(d–i)] for a specimen of the S1 material, subjected to a $CSR = 0.12$, and $\sigma'_{v0} = 300$ kPa. (Similar plots for all CSS tests are presented in the Figs. S29–S56.) Before discussing the patterns, the following variables are defined: the rate of shear strain accumulation ($\Delta\gamma$), which represents the difference in the maximum axial strains during two consecutive

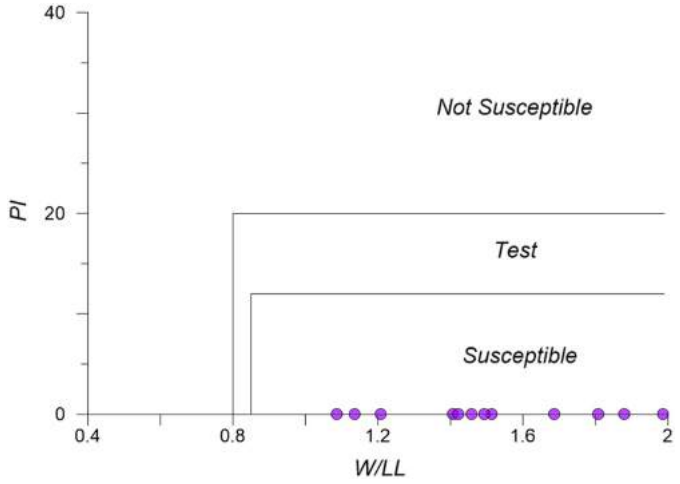

Fig. 12. Assessment of the liquefaction response for gradations S1, S2, and S3 using the Bray and Sancio (2006) criterion.

cycles; the stiffness index (δ_S) (Idriss et al. 1978; Vucetic and Mortezaie 2015), defined as the secant shear modulus of the Nth stress–strain loop (G_{SN}), divided by the secant shear modulus of the first cycle (G_{S1}); S_N, which is the area of the Nth stress–strain loop; ΔG_{SN}, which is the change in the secant shear modulus between two consecutive cycles; ΔR_{u-N}, defined as the change in the maximum pore pressure ratio between two consecutive cycles; VEDR $= \frac{S_N}{X_N}$, which represents the viscous energy damping ratio defined by Ke et al. (2019), where S_N was already defined and X_N is the area of the circumscribed rectangle to the Nth stress–strain loop; and δ_T, which is the tangent stiffness index, calculated as the tangent shear modulus in the Nth cycle normalized by its counterpart on the first cycle. The variation in these parameters versus the number of cycles is shown in Figs. 13(d–h). Three stages can be defined by inspecting the variation of these parameters: (1) stage 1 (cycles 1 to 25), where there is a linearly decreasing trend for δ_S and δ_T, a close to increasing linear trend for VEDR, and $\Delta\gamma$, S_N, ΔG_{SN}, and ΔR_{u-N} are almost constant. A typical stress–strain loop during this stage is shown in Fig. 13(i) (cycle 25). (2) Stage 2 (cycles 25 to 34) is characterized by an increasing rate of change for all the parameters and a region of maximum curvature, and the triggering of liquefaction is expected to occur close to the end of this stage (a typical stress–strain loop in this stage is shown in Fig. 13(i); see cycle 34). (3) The start of stage 3 is marked by a change in curvature of δ_S and δ_T, a faster increase in S_N, a saturation of VEDR (i.e., a maximum value is reached), and a significant increase in shear strains. These patterns indicate that there is no more room for stiffness degradation or pore pressure increase, and the sample is freely developing large strains; Fig. 13(i) shows a typical stress–strain loop in this stage (see cycle 37). The beginnings of stages 2 and 3 are also indicated in the test results in Figs. 13(a–c), showing consistency with the observed patterns.

The aforementioned patterns can be used to define the triggering of cyclic liquefaction. The current practice uses strain-amplitude criteria; for example, the development of a 3.75% single amplitude (SA) axial strain has been suggested in NRC (1985) and also used in previous mine tailings studies (e.g., Wijewickreme et al. 2005a); other studies on mine tailings have also used 3% SA axial strain as a criterion (e.g., Suazo et al. 2016). In this context, Wijewickreme and Soysa (2016) stated that strain-based criteria are arbitrary and suggested an approach based on the shape of stress–strain loops, introducing the concept of a "kink" point, which indicates the transition from what they denominated "X" to "Y" stress–strain loops. An "X" loop does not show a change in curvature during loading and unloading, whereas a "Y" loop shows a change in curvature [Fig. 13(f)]. Different potential alternatives to define the onset of liquefaction based on the parameters previously discussed can be explored. For instance, we consider the number of cycles corresponding to the point of maximum curvature in $\Delta\gamma$, δ, S_N, and the peak in ΔG_{SN}, ΔR_u, and VEDR (Fig. 13). We denominate the number of cycles associated with these options as NL_1, NL_2, NL_3, NL_4, NL_5, and NL_6. Fig. 14(a) shows the comparison of NL_1, NL_2, NL_3, NL_4, NL_5, and NL_6, versus the number of cycles evaluated with the Wijewickreme and Soysa (2016) "kink" point criterion, denominated as NL_{WS} [Fig. 13(f) shows a typical assessment of NL_{WS}]. In general, the number of cycles evaluated from different criteria is consistent, but NL_4, NL_5, and NL_6 are relatively more consistent with NL_{WS}. Thus, we recommend assessing the number of cycles for cyclic liquefaction by using the ΔG_{SN}, ΔR_u, or VEDR criteria. Figs. 14(b–d) show histograms of the SA axial strain at which liquefaction occurs using the ΔG_{SN}, ΔR_u, and VEDR criteria. It can be observed that liquefaction can occur at a range of SA strain values—and, in most cases, at SA strains below 3.75%. It is also important to highlight that the proposed ΔG_{SN}, ΔR_u, or VEDR criteria are based on patterns observed on the cyclic response, and, hence, they are not arbitrary, such as a criterion based on a fixed SA strain. Last, the proposed criteria can be automated; this overcomes one of the issues with the NL_{WS}-based criterion, which requires a manual inspection of different stress–strain loops.

Liquefaction Resistance Curves

Fig. 15 shows liquefaction resistance curves (i.e., CSR versus the number of cycles to reach liquefaction using the NL_6 criterion previously discussed) for materials S1, S2, and S3 under different σ'_{v0} values in the range from 50 to 1,000 kPa. Interestingly, there is a significant difference in the liquefaction resistance curves for the S1 material (Fig. 15) for different σ'_{v0}. This difference decreases for the S2 material [Fig. 15(b)] and decreases further for the S3 material [Fig. 15(c)]. In addition, the liquefaction resistance curves move upward as σ'_{v0} increases, which is in contrast with the typical trends observed for clean sands that show a downward movement as σ'_{v0} increases (e.g., Vaid et al. 2001). However, the key difference is that sands often have low compressibility, whereas mine tailings are comparatively more compressible (see compressibility section). Hence, there are two competing effects when σ'_{v0} is increased in mine tailings, namely, (1) an enhancement of a contractive response due to the stress increment; and (2) an enhancement of a dilative response due to stress densification. In addition to properties intrinsic to each material (i.e., particle properties and gradation), these competing effects mark the relative position of the liquefaction resistance curves in Fig. 15. These competing effects have also been observed in a few previous studies for mine tailings and fine-grained natural soils (Wijewickreme et al. 2005a, b; Suazo et al. 2016; Wijewickreme et al. 2019). Another factor that might influence these trends is the relative position of the consolidation lines and the CSL. For instance, in the case of the S3 gradation, these lines are reasonably parallel over a range of stresses (Fig. 6), suggesting a "clay-type" behavior for which previous studies have shown that liquefaction resistance curves are not significantly affected by changes in stresses (e.g., Wijewickreme et al. 2005a; Zergoun and Vaid 1994; Atkinson and Bransby 1978). This is in contrast with the observations for S1, where the consolidation lines and CSL are not parallel (Fig. 6), and a larger difference in the liquefaction resistance curves for different stress levels is observed. Last, the

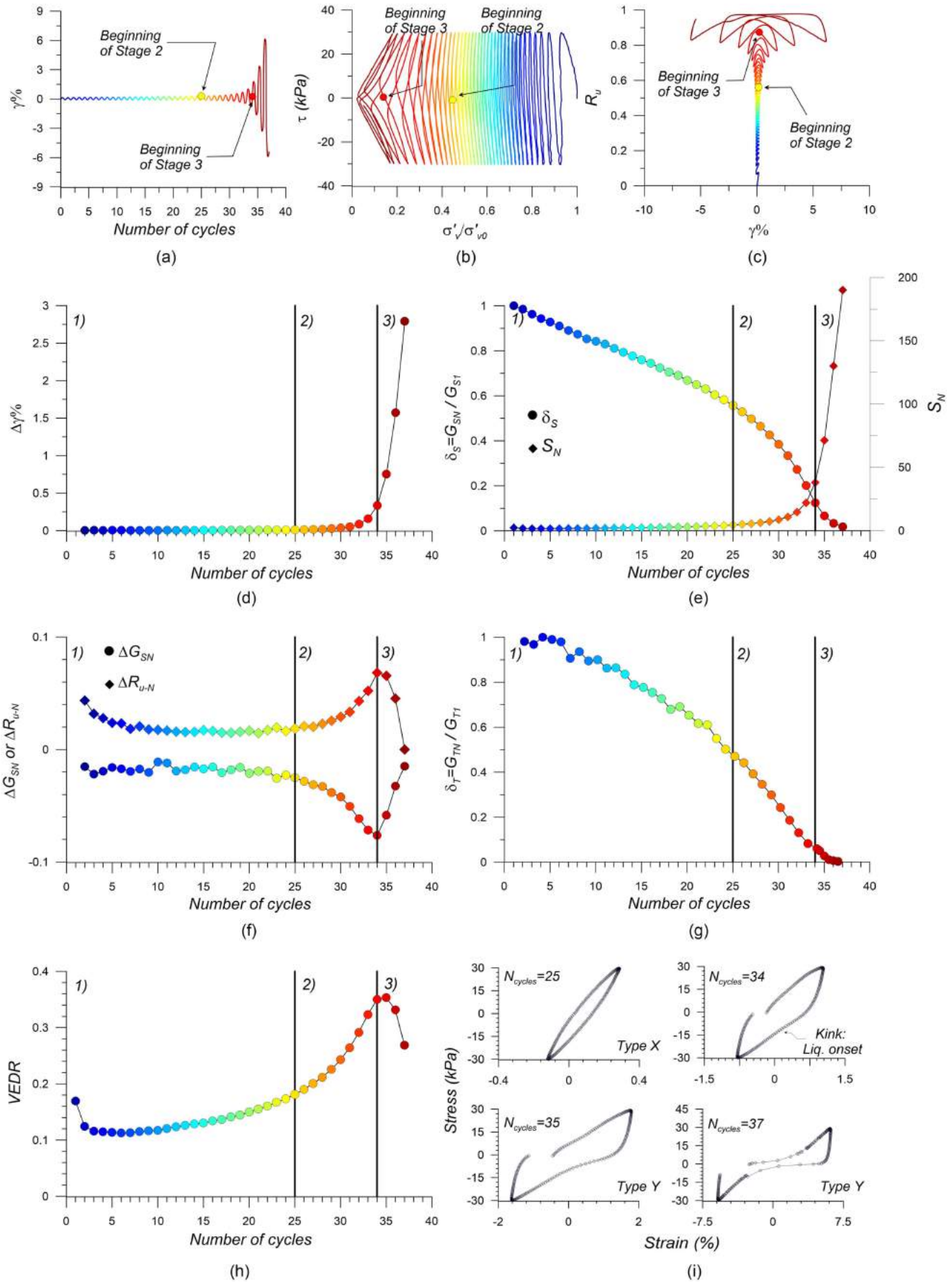

Fig. 13. CSS test results for material S1 at $\sigma_{v0} = 300$ kPa and $CSR = 0.10$, showing (a) number of cycles versus γ (%); (b) σ'_v versus τ; and (c) γ (%) versus R_u. The number of cycles versus (d) $\Delta\gamma$; (e) δ_S and S_N; (f) ΔG_{SN} and ΔR_{u-N}; (g) δ_T; and (h) VEDR. (i) Typical assessment of stress–strain loops according to Wijewickreme and Soysa (2016).

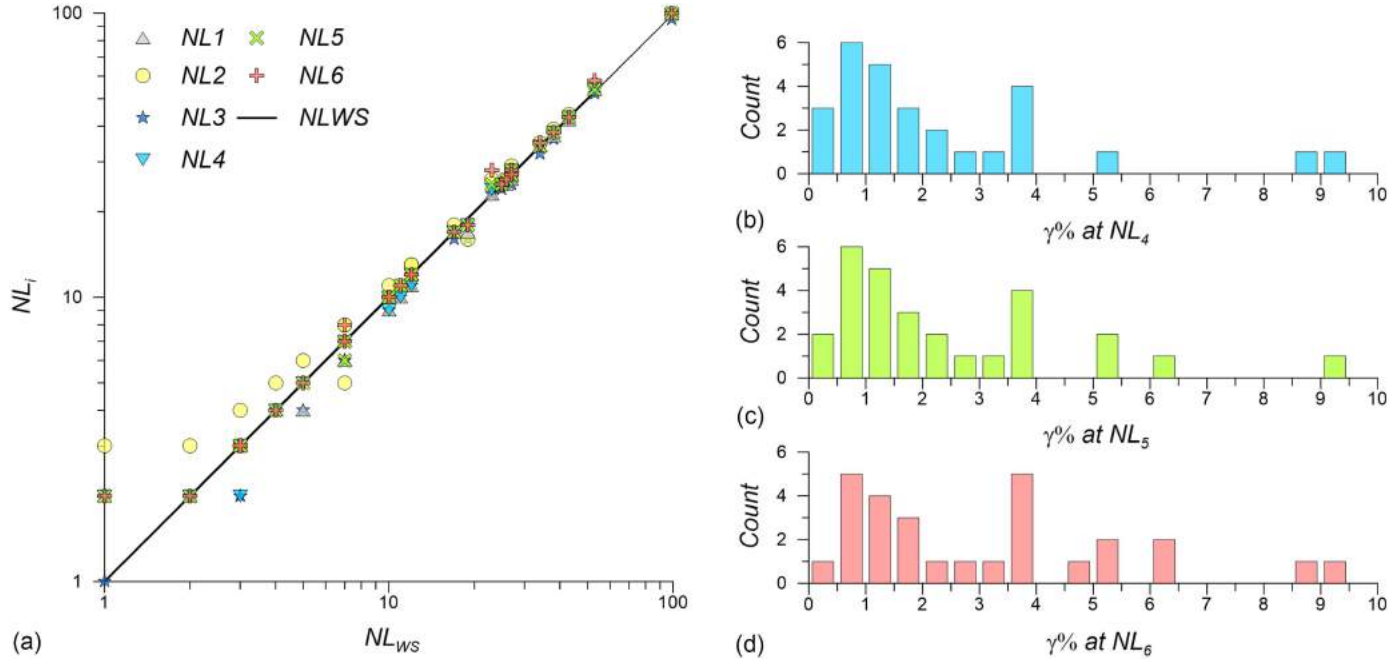

Fig. 14. (a) Comparison of the number of cycles to trigger liquefaction using different criteria proposed in this study against the (Wijewickreme and Soysa 2016) criterion; histograms for the SA strain levels associated with the (b) NL_4; (c) NL_5; and (d) NL_6 criteria.

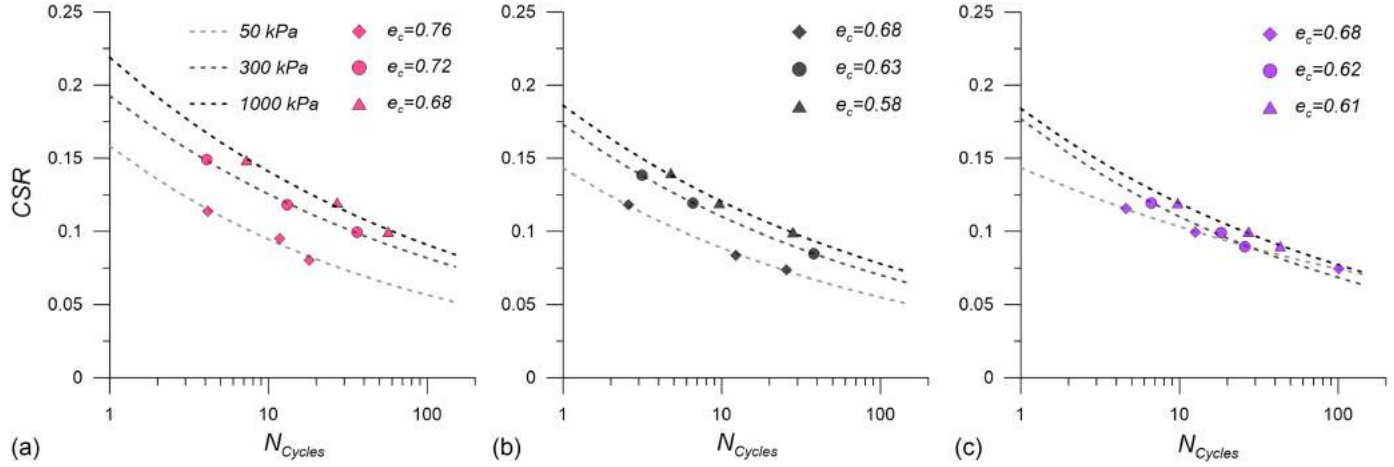

Fig. 15. Liquefaction resistance curves for gradations: (a) S1; (b) S2; and (c) S3.

relative positions of the curves in Fig. 15 also suggest that the initial state alone may not be a robust indicator of cyclic resistance. For instance, putting uncertainties aside (i.e., assuming the same K_0, and that the CSL lines in Fig. 6 are applicable to plane strain conditions, representative of CSS tests), and considering the gradation S1, the CSS tests at 1,000 kPa show a higher CRR_{15} (i.e., CRR at 15 cycles) than the tests at 50 kPa; however, the overall ψ_0 would be more negative for the tests at 50 kPa. This is in contrast to what would be expected if ψ_0 were robust in explaining cyclic resistance. Similar limitations in ψ_0 for representing the cyclic resistance have also been highlighted by Gu et al. (2015). Similar patterns could also be observed in Fraser River sand data (Jefferies and Been 2015), and results from DEM simulations (Rahman et al. 2021), when inspecting data at a broad range of stresses, as considered in this study. More research is warranted to find state-based metrics to explain cyclic resistance.

Postcyclic Behavior

Postcyclic reconsolidation volumetric strains (ε_{v-pc}) are compared against the maximum pore-water pressure ratios ($R_{u-\max}$) and the maximum cyclic shear strains ($\gamma_{\max}$) during cyclic loading in Figs. 16(a and b). The comparisons are motivated by previous studies on natural silty soils that inspected the relationships between these parameters (e.g., Wijewickreme and Sanin 2010; Jana and Stuedlein 2021) and are useful in putting our results for mine tailings in context. Wijewickreme and Sanin (2010) found a strong correlation between ε_{v-pc} and $r_{u-\max}$ regardless

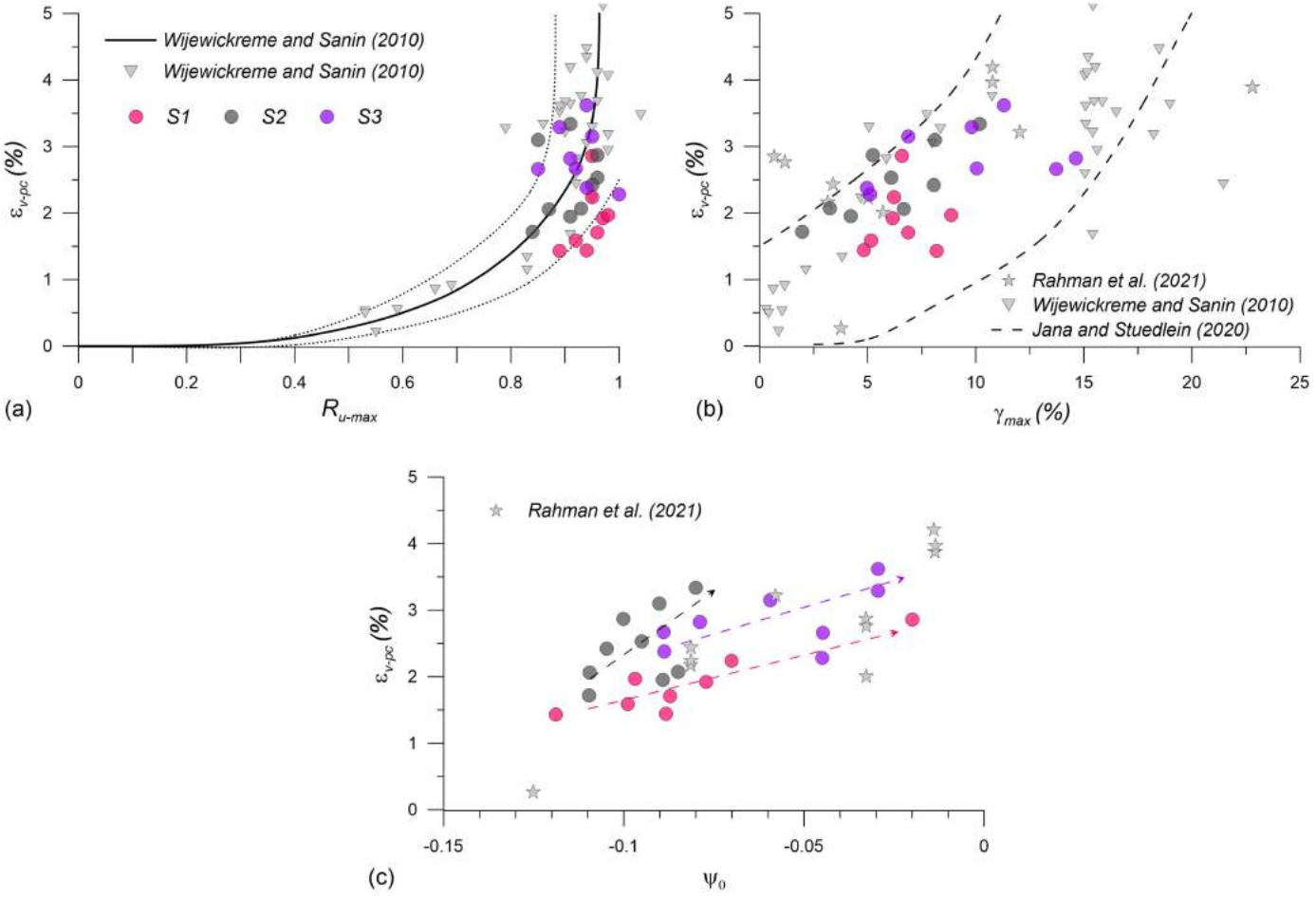

Fig. 16. Postcyclic behavior for the examined mine tailings: (a) ε_{v-pc} versus $r_{u-\max}$; (b) ε_{v-pc} versus $\gamma_{\max}$; and (c) ε_{v-pc} versus ψ_0.

of the initial state, with large ε_{v-pc} values (~1.5% to 5%) developing when $r_{u-\max} > 0.8$. Fig. 16(a) shows that the $\varepsilon_{v-pc} - r_{u-\max}$ for the S1, S2, and S3 gradations are consistent with the limits proposed by Wijewickreme and Sanin (2010) based on Fraser River silty soils. Fig. 16(b) shows the variation between ε_{v-pc} and $\gamma_{\max}$, including the upper and lower limits proposed by Jana and Stuedlein (2021) based on natural silts from Portland and the data from Wijewickreme and Sanin (2010). Again, it can be observed that the results for mine tailings are generally consistent with the upper and lower limits from Jana and Stuedlein (2021) and follow the general trends observed in Wijewickreme and Sanin (2010). Thus, our results suggest that the limits proposed by Wijewickreme and Sanin (2010) and Jana and Stuedlein (2021) for natural silty soils also apply to mine tailings. Last, Fig. 16(c) shows how ε_{v-pc} varies with ψ_0 before cyclic loading, along with DEM-based results from Rahman et al. (2021). Even though there is a significant scatter, it can be observed that there is a trend for ε_{v-pc} to increase as ψ_0 becomes more positive, which is expected as a more positive ψ_0 enhances a contractive response.

Cyclic Liquefaction Triggering—Field Scale

In this section, we evaluate different CPT-based procedures for liquefaction triggering assessment. Since several state-of-practice approaches use FC (e.g., Boulanger and Idriss 2016) or I_c (e.g., Robertson 2010, 2021), we first inspected the relationship between FC and I_c for the mine tailings being investigated. FC was estimated from the recovered samples and I_c from the CPTs. Fig. 17 shows the variation in I_c versus FC, also presenting the I_c–FC relationships from Robertson and Wride (1998) and Boulanger and Idriss (2016) for comparison purposes. These I_c–FC relationships were developed for silty sands with FC up to ~35% and, in principle, should not be applied to mine tailings; however, the extrapolation of the Boulanger and Idriss (2016)

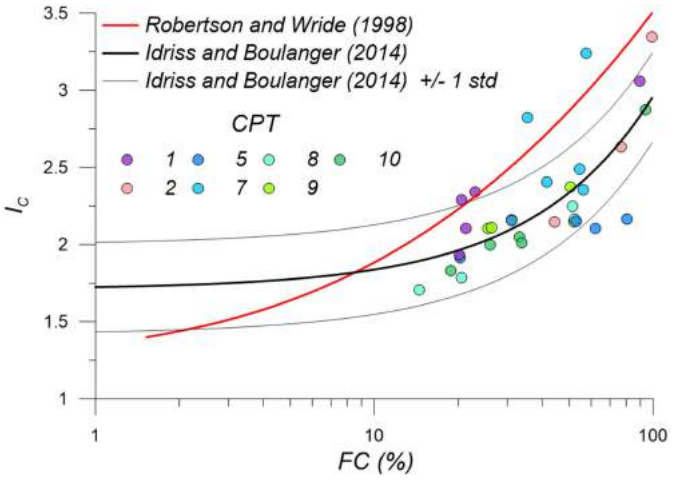

Fig. 17. I_c versus FC compared against the relationships from Robertson and Wride (1998) and Boulanger and Idriss (2014).

J. Geotech. Geoenviron. Eng., 2023, 149(5): 04023021

relationship seems to capture the observed I_c–FC data well. In contrast, the Robertson and Wride (1998) relationship seems to underestimate the FC for a given I_c. Engineers often use the I_c–FC relationship from Boulanger and Idriss (2016) when their liquefaction triggering procedure is applied to mine tailings. This seems adequate for the mine tailings being examined, but it should be explored further for other tailings in the future. In the following, we will use the I_c–FC relationship from Boulanger and Idriss (2016) when a I_c–FC conversion is needed. Given the large FC in the mine tailings being examined, we will use the ΔQ procedure recently proposed by Saye et al. (2021) to put in context the outcomes from the Boulanger and Idriss (2016) and Robertson and Wride (1998) methods, which we will denominate BI16 and RW98, respectively. Of note, the BI16 and RW98 methods have been formulated for silty sands with FC up to ~35% and, in principle, are not strictly applicable to mine tailings with large FC but are commonly used in tailings engineering. The logic in using the ΔQ procedure [where ΔQ is defined as $(Q_t + 10)/(f_s/\sigma'_v + 0.67)$ and $Q_t = q_t - \sigma_v/\sigma'_v$] as the basis for comparisons is that it is applicable to a broad range of soils with contrasting compressibility regardless of their FC through interactions between Q_t and f_s (Saye et al. 2021). The ΔQ method brings compressibility effects directly through f_s, which, as previously discussed, is important for mine tailings. Toward this end, we use the receiver operating characteristic (ROC) curve, which is a machine learning method that scores the performance of classification procedures (e.g., BI16 and RW98), to classify data with known categories (e.g., liquefaction versus nonliquefaction). More details on ROC can be found in Fawcett (2006) and Maurer et al. (2015). We consider the liquefaction/nonliquefaction outcomes from the ΔQ procedure as the baseline reference to compare the BI16 and RW98 methods against the ΔQ approach. In addition, the evaluations are performed for different PGA levels, namely 0.10, 0.30, and 0.50 g. The Supplemental Materials section shows the details for the calculations in Figs. S57–S66. Figs. 18(a–c) present the ROC curves for the BI16 and RW98 procedures, considering different PGAs and all the CPTs in Fig. 2.

When using ROC curves, the area under the curve (AUC) is used to assess the classification accuracy. When the AUC is larger (the maximum value is 1), the ROC curve is closer to the top left corner of the axes in Fig. 18, and the performance of a classification method is judged to be better. BI16 consistently performs more similarly to ΔQ than RW98 for PGA values lower than 0.3 g. For instance, the AUC values from the BI16 method range from 0.75 to 0.92 (with an average of 0.84), whereas the AUC values for the RW98 procedure vary from 0.71 to 0.88 (with an average of 0.79). Even though BI16 performs more similarly to ΔQ in this PGA range, the AUC values for BI16 and RW98 are large, indicating a comparable performance between ΔQ, BI16, and RW98. As the PGA increases (i.e., values larger than 0.3 g), the AUC values for the BI16 and RW98 methods are larger (AUC > 0.93), indicating an even more comparable performance when compared against ΔQ, where any procedure predicts liquefaction triggering. The comparable performance between ΔQ, BI16, and RW98 may

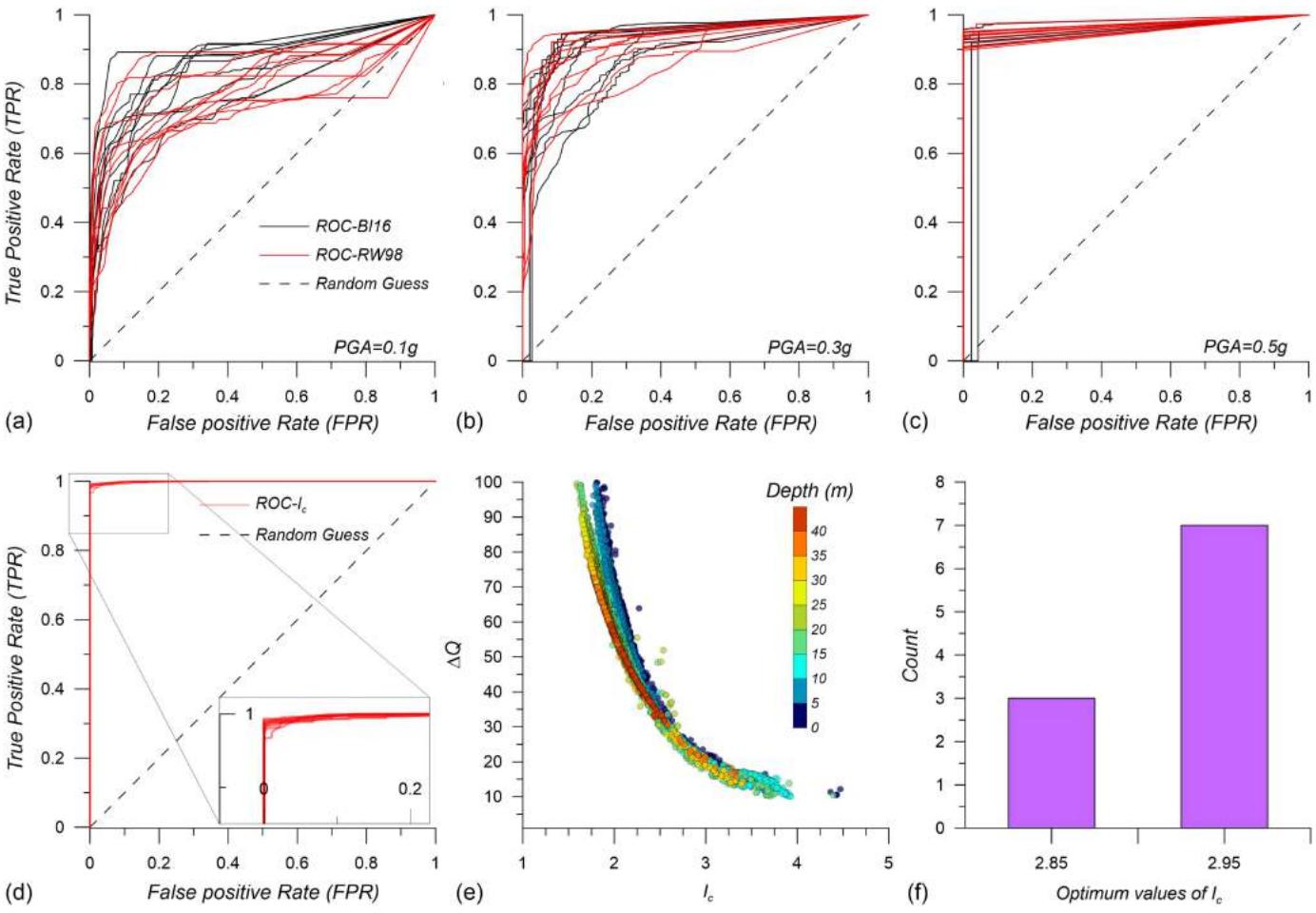

Fig. 18. ROC curves for BI16 and RW98 considering: (a) PGA = 0.1 g; (b) PGA = 0.3 g; (c) PGA = 0.5 g; (d) ROC curve for the ΔQ method considering different I_c values; (e) ΔQ vs I_c; and (f) Histogram of optimum I_c.

J. Geotech. Geoenviron. Eng., 2023, 149(5): 04023021

be attributed to the fact that ΔQ explicitly adds compressibility information through f_s. However, compressibility information is also indirectly considered in the BI16 and RW98 procedures through I_c–FC or I_c relationships, which incorporate f_s.

The ΔQ procedure also indicates that for ΔQ values lower than 20, the susceptibility to significant cyclic softening and liquefaction-like behavior is not significant (Saye et al. 2021). Hence, we use this threshold to label as susceptible/nonsusceptible the CPT data, treating these labels as the baseline reference to evaluate the performance of using an I_c threshold as commonly done in the BI16 and RW98 methods. Again, we use ROC curves where different I_c values are used for constructing the curves, with the results presented in Fig. 18(d). The large AUC values (AUC > 0.99) indicate that the I_c-based and ΔQ-based procedures are comparable in identifying susceptibility for the mine tailings being examined. This can also be illustrated through the strong correlation between ΔQ and I_c, which is shown for an illustrative CPT in Fig. 18(e). Last, Fig. 18(f) shows the histogram of the optimal I_c values estimated by the ROC procedure for comparable performance against the ΔQ procedure. The I_c values vary from 2.84 to 2.97 with an average I_c of 2.9. This estimate contrasts with the common I_c value of 2.6 used in engineering practice (e.g., Boulanger and Idriss 2016), but it is closer to the I_c value of 3.0 recommended by Robertson (2021) based on the recent case histories of TSF failures, e.g., the Fundao dam failure Morgenstern et al. (2016) and Feijao dam failure on Brumadinho Robertson et al. (2019). Thus, our results suggest that an I_c value of 2.9 is more representative for mine tailings; we recommend inspecting this finding using other mine tailings in the future.

Conclusions

Mine tailings are geologically young materials, with angular grains rather than subrounded and often with lower proportions of quartz than many natural soils, which makes the characterization of their response to static and cyclic solicitations challenging. In this context, this study contributes to the understanding of the mechanical response of mine tailings by presenting salient observations of the static and cyclic responses of three different copper mine tailings gradations, which include the following.

1. The results from oedometer and isotropic consolidation tests for the examined tailings and data from previous studies suggest that I_v seems appropriate to characterize the compressibility of mine tailings regardless of their ore source.
2. V_s measurements in the field and laboratory suggest fabric differences across these scales, which might be associated with the limitations of moist tamping on reconstituting *in situ* fabrics. In addition, the $G_{\max}-p$ scaling of the examined tailings is quite different compared to sands; hence, a model modified from Payan and Chenari (2019) was proposed. This model should be verified in future studies.
3. The theoretical particle size distributions that promote packing proposed by Lade et al. (1998) are useful in understanding general trends for the location of the CSL of mine tailings, highlighting the role of the relative proportions of particle sizes and particle properties.
4. The tailings examined in this study can suffer static and cyclic liquefaction regardless of their fine contents. Hence, our results support the idea that FC is not a robust proxy to assess liquefaction resistance. Instead, mechanical-based parameters that reflect the particle properties and proportion of particle sizes (e.g., Γ, λ_e, M_{tc}, N, χ, and $G_{\max}$) should be used.
5. Commonly used strain-based criteria are not robust for identifying the onset of cyclic liquefaction in the examined tailings. Instead, we propose different criteria based on mechanistic descriptors. Specifically, we recommend using criteria based on ΔG_{SN}, ΔR_u, or VEDR.
6. The cyclic response of the examined mine tailings is affected by coupled stress-compressibility. In addition, their posttriggering cyclic response contrasts with the patterns often observed in natural sands, i.e., the increment of strains accumulated after triggering is not stable. In terms of post-cyclic patterns, the observed trends fall within the range observed for natural silts.
7. Using the ΔQ procedure as a baseline (as it applies to a range of soils regardless of their FCs), we find that the RW98 and BI16 methods formulated for silty sands with FC up to ~40% perform similarly to ΔQ for the examined tailings, especially for large PGAs associated with common design scenarios. We suggest that this is the case because these methods (ΔQ, RW98, and BI16) directly or indirectly include compressibility information.
8. The efficiency for identifying liquefaction susceptibility using I_c is comparable to that of the ΔQ procedure for the tailings examined in this study. In addition, the optimum I_c threshold consistent with ΔQ equal to 20 was identified as 2.9.

Appendix. Norsand Calibrated Parameters for the Examined Mine Tailings Gradation S1, S2, and S3

Material	S1	S2	S3
CSL			
Γ/λ_e	1.013/0.045	0.876/0.033	0.86/0.033
$a/b/c$	0.924/0.096/0.421	0.865/0.123/0.275	0.742/0.022/0.856
Elasticity			
G_0	125	95	90
B	0.58	0.63	0.69
v	0.15	0.15	0.15
Plasticity			
M_{tc}	1.55	1.54	1.49
N	0.3	0.3	0.3
χ_{tc}	4	4	4
H_0	253	117	108
H_ψ	1,617	984	1,206

Note: a = void ratio corresponding to a mean pressure equal to 0 kPa; B = exponent of the power-law ($G_{\max} = G_0 \cdot (p/P_a)^B$) elasticity; b = parameter of the power-law (curved CSL) expression; c = exponent of the power-law expression; G_0 = reference value of the shear modulus at the reference pressure ($P_a = 100$ kPa); $\boldsymbol{H_0}$ = hardening parameter; $\boldsymbol{H_\psi}$ = hardening parameter; $\boldsymbol{M_{tc}}$ = critical stress ratio; N = volumetric coupling; $\boldsymbol{\chi_{tc}}$ = state-dilatancy parameter; Γ = void ratio corresponding to a mean pressure equal to 1 kPa; $\boldsymbol{\lambda_e}$ = slope of the critical state line; and v = Poisson's ratio.

Data Availability Statement

Some or all data, models, or code generated or used during this study are available from the corresponding author by request.

Acknowledgments

This study has been funded by the National Science Foundation (NSF) under the CMMI 2013947 project. We also acknowledge the financial support provided by the Pronabec program of the Peruvian government for the first author. Finally, we also thank

Mr. Terry Eldridge for providing information on Supplemental Materials S1–S3.

Supplemental Materials

Figs. S1–S66 are available online in the ASCE Library (www.ascelibrary.org).

References

Anderson, C., and T. Eldridge. 2011. "Critical state liquefaction assessment of an upstream constructed tailings sand dam." *Tailings Mine Waste* 2010 (1): 101–112. https://doi.org/10.1201/b10569-15.

Atkinson, J. H., and P. L. Bransby. 1978. *The mechanics of soil: An introduction to critical state soil mechanics*. New York: McGraw-Hill.

Bedin, J., F. Schnaid, A. V. Da Fonseca, and L. D. M. Costa Filho. 2012. "Gold tailings liquefaction under critical state soil mechanics." *Géotechnique* 62 (3): 263–267.

Been, K. 2016. "Characterizing mine tailings for geotechnical design." In *Geotechnical and geophysical site characterisation*. Sydney, Australia: Australian Geomechanics Society.

Been, K., and M. G. Jefferies. 1985. "A state parameter for sands." *Géotechnique* 35 (2): 99–112. https://doi.org/10.1680/geot.1985.35.2.99.

Been, K., and G. C. Sills. 1981. "Self-weight consolidation of soft soils: An experimental and theoretical study." *Géotechnique* 31 (4): 519–535. https://doi.org/10.1680/geot.1981.31.4.519.

Boulanger, R. W., and I. M. Idriss. 2014. *CPT and SPT based liquefaction triggering procedures*. Rep. No. UCD/CGM-14/01. Davis, CA: Univ. of California.

Boulanger, R. W., and I. M. Idriss. 2016. "CPT-based liquefaction triggering procedure." *J. Geotech. Geoenviron. Eng.* 142 (2): 04015065. https://doi.org/10.1061/(ASCE)GT.1943-5606.0001388.

Bray, J. D., and R. B. Sancio. 2006. "Assessment of the liquefaction susceptibility of fine-grained soils." *J. Geotech. Geoenviron. Eng.* 132 (9): 1165–1177. https://doi.org/10.1061/(ASCE)1090-0241(2006)132:9(1165).

Burland, J. B. 1990. "On the compressibility and shear strength of natural clays." *Géotechnique* 40 (3): 329–378. https://doi.org/10.1680/geot.1990.40.3.329.

Carrera, A., M. Coop, and R. Lancellotta. 2011. "Influence of grading on the mechanical behaviour of Stava tailings." *Géotechnique* 61 (11): 935–946. https://doi.org/10.1680/geot.9.P.009.

Chang, N., G. Heymann, and C. Clayton. 2011. "The effect of fabric on the behaviour of gold tailings." *Géotechnique* 61 (3): 187–197. https://doi.org/10.1680/geot.9.P.066.

Cho, G.-C., J. Dodds, and J. C. Santamarina. 2006. "Particle shape effects on packing density, stiffness, and strength: Natural and crushed sands." *J. Geotech. Geoenviron. Eng.* 132 (5): 591–602. https://doi.org/10.1061/(ASCE)1090-0241(2006)132:5(591).

Chu, J., and W. K. Leong. 2002. "Effect of fines on instability behaviour of loose sand." *Géotechnique* 52 (10): 751–755. https://doi.org/10.1680/geot.2002.52.10.751.

Crowder, J. J. 2004. "Deposition, consolidation, and strength of a non-plastic tailings paste for surface disposal." Ph.D. thesis, Dept. of Civil Engineering, Univ. of Toronto.

Dafalias, Y. F., and M. T. Manzari. 2004. "Simple plasticity sand model accounting for fabric change effects." *J. Eng. Mech.* 130 (6): 622–634. https://doi.org/10.1061/(ASCE)0733-9399(2004)130:6(622).

Daliri, F., P. Simms, and S. Sivathayalan. 2015. "Discussion of 'Stiffness and strength governing the static liquefaction of tailings' by F. Schnaid, J. Bedin, A. J. P. Viana da Fonseca, and L. de Moura Costa Filho." *J. Geotech. Geoenviron. Eng.* 141 (9): 07015023. https://doi.org/10.1061/(ASCE)GT.1943-5606.0001328.

De Alba, P., K. Baldwin, V. Janoo, G. Roe, and B. Celikkol. 1984. "Elastic-wave velocities and liquefaction potential." *Geotechn. Test. J.* 7 (2): 77–87.

Fawcett, T. 2006. "An introduction to ROC analysis." *Pattern Recognition Lett.* 27 (8): 861–874. https://doi.org/10.1016/j.patrec.2005.10.010.

Fourie, A. B., and G. Papageorgiou. 2001. "Defining an appropriate steady state line for Merriespruit gold tailings." *Can. Geotech. J.* 38 (4): 695–706. https://doi.org/10.1139/t00-111.

Fourie, A. B., and L. Tshabalala. 2005. "Initiation of static liquefaction and the role of K0 consolidation." *Can. Geotech. J.* 42 (3): 892–906. https://doi.org/10.1139/t05-026.

GEER (Geo-Engineering Extreme Events Reconnaissance Association). 2010. "Dams, levees, and mine tailings dams." In *Turning disaster into knowledge: Geo-engineering reconnaissance of the 2010 Maule, Chile Earthquake*, 204–226. Liège, Belgium: GEER.

Geremew, A. M., and E. K. Yanful. 2013. "Dynamic properties and influence of clay mineralogy types on the cyclic strength of mine tailings." *Int. J. Geomech.* 13 (4): 441–453. https://doi.org/10.1061/(ASCE)GM.1943-5622.0000227.

Gill, S. S. 2019. *Geotechnical properties of tailings: Effect of fines content*. Toronto, Canada: Univ. of Toronto.

Goudarzy, M., M. M. Rahman, D. König, and T. Schanz. 2016. "Influence of non-plastic fines content on maximum shear modulus of granular materials." *Soils Found.* 56 (6): 973–983. https://doi.org/10.1016/j.sandf.2016.11.003.

Gu, X. Q., J. Yang, M. S. Huang, and G. Y. Gao. 2015. "Bender element tests in dry and saturated sand: Signal interpretation and result comparison." *Soils Found.* 55 (5): 951–962. https://doi.org/10.1016/j.sandf.2015.09.002.

Hu, L., H. Wu, L. Zhang, P. Zhang, and Q. Wen. 2017. "Geotechnical properties of mine tailings." *J. Mater. Civ. Eng.* 29 (2): 04016220. https://doi.org/10.1061/(ASCE)MT.1943-5533.0001736.

Idriss, I. M., R. Dobry, and R. D. Singh. 1978. "Nonlinear behavior of soft clays during cyclic loading." *J. Geotech. Eng. Div.* 104 (12): 1427–1447. https://doi.org/10.1061/AJGEB6.0000727.

James, M., M. Aubertin, D. Wijewickreme, and G. W. Wilson. 2011. "A laboratory investigation of the dynamic properties of tailings." *Can. Geotech. J.* 48 (11): 1587–1600. https://doi.org/10.1139/t11-060.

Jana, A., and A. W. Stuedlein. 2021. "Monotonic, cyclic, and postcyclic responses of an alluvial plastic silt deposit." *J. Geotech. Geoenviron. Eng.* 147 (3): 04020174. https://doi.org/10.1061/(ASCE)GT.1943-5606.0002462.

Jefferies, M. 2022. "Improving governance will not be sufficient to avoid dam failures." *Proc. Inst. Civ. Eng. Geotech. Eng.* 175 (2): 166–180. https://doi.org/10.1680/jgeen.21.00105.

Jefferies, M. G. 1993. "Nor-Sand: A simple critical state model for sand." *Géotechnique* 43 (1): 91–103. https://doi.org/10.1680/geot.1993.43.1.91.

Jefferies, M. G., and K. Been. 2015. *Soil liquefaction: A critical state approach*. 2nd ed. Boca Raton, FL: CRC Press.

Ke, X., J. Chen, and Y. Shan. 2019. "A new failure criterion for determining the cyclic resistance of low-plasticity fine-grained tailings." *Eng. Geol.* 261 (Sep): 105273. https://doi.org/10.1016/j.enggeo.2019.105273.

Kossoff, D., W. E. Dubbin, M. Alfredsson, S. J. Edwards, M. G. Macklin, and K. A. Hudson-Edwards. 2014. "Mine tailings dams: Characteristics, failure, environmental impacts, and remediation." *Appl. Geochem.* 51 (14): 229–245. https://doi.org/10.1016/j.apgeochem.2014.09.010.

Ladd, R. 1978. "Preparing test specimens using undercompaction." *Geotech. Test. J.* 1 (1): 16. https://doi.org/10.1520/GTJ10364J.

Lade, P., C. Liggio, and J. Yamamuro. 1998. "Effects of non-plastic fines on minimum and maximum void ratios of sand." *Geotech. Test. J.* 21 (4): 336. https://doi.org/10.1520/GTJ11373J.

Lade, P. V., and J. A. Yamamuro. 1997. "Effects of non-plastic fines on static liquefaction of sands." *Can. Geotech. J.* 34 (Jun): 918–928. https://doi.org/10.1139/t97-052.

Li, G., Y.-J. Liu, C. Dano, and P.-Y. Hicher. 2014. "Grading-dependent behavior of granular materials: From discrete to continuous modeling." *J. Eng. Mech.* 141 (6): 04014172. https://doi.org/10.1061/(ASCE)EM.1943-7889.0000866.

Li, W. 2017. "The mechanical behaviour of tailings." Ph.D. thesis, Dept. of Architecture and Civil Engineering, City Univ. of Hong Kong.

Li, W., and M. R. Coop. 2019. "Mechanical behavior of Panzhihua iron tailings." *Can. Geotech. J.* 56 (3): 420–435. https://doi.org/10.1139/cgj-2018-0032.

Li, W., M. R. Coop, K. Senetakis, and F. Schnaid. 2018. "The mechanics of a silt-sized gold tailing." *Eng. Geol.* 241 (Jul): 97–108. https://doi.org/10.1016/j.enggeo.2018.05.014.

Li, X. S., and Y. F. Dafalias. 2012. "Anisotropic critical state theory: Role of fabric." *J. Eng. Mech.* 138 (3): 263–275. https://doi.org/10.1061/(ASCE)EM.1943-7889.0000324.

Macedo, J., J. Bray, S. Olson, C. Bareither, and C. Arnold. 2020. "TAILENG mine tailings database." In *Proc., Tailings and Mine Waste 2020 Conf.* Keystone, Colorado. Vancouver, BC, Canada: Univ. of British Columbia.

Macedo, J., and A. Petalas. 2019. "Calibration of two plasticity models against the static and cyclic response of tailings materials." In *Proc., Tailings and Mine Waste*. Vancouver, BC, Canada: Univ. of British Columbia.

Macedo, J., and L. Vergaray. 2021. "Properties of mine tailings for static liquefaction assessment." *Can. Geotech. J.* 59 (5): 667–687. https://doi.org/10.1139/cgj-2020-0600.

Maurer, B. W., R. A. Green, M. Cubrinovski, and B. A. Bradley. 2015. "Assessment of CPT-based methods for liquefaction evaluation in a liquefaction potential index framework." *Géotechnique* 65 (5): 328–336. https://doi.org/10.1680/geot.SIP.15.P.007.

McGeary, R. K. 1961. "Mechanical packing of spherical particles." *J. Am. Ceram. Soc.* 44 (10): 513–522. https://doi.org/10.1111/j.1151-2916.1961.tb13716.x.

Morgenstern, N. R. 2018. "Geotechnical risk, regulation, and public policy—The sixth Victor de Mello lecture." *Soils Rocks* 41 (2): 107–129. https://doi.org/10.28927/SR.412107.

Morgenstern, N. R., M. Jefferies, D. Zyl, and J. Wates. 2019. "Independent technical review board." Accessed April 8, 2021. https://www.newcrest.com/sites/default/files/2019-10/190417_Report%20on%20NTSF%20Embankment%20Failure%20at%20Cadia%20for%20Ashurst.pdf.

Morgenstern, N. R., S. G. Vick, C. B. Viotti, and B. D. Watts. 2016. "Fundao tailings dam review panel." Accessed April 16, 2021. http://fundaoinvestigation.com/the-panel-report/.

National Research Council. 1985. *Liquefaction of soils during earthquakes*. Washington, DC: The National Academies Press.

Olson, S. M., and T. D. Stark. 2003. "Use of laboratory data to confirm yield and liquefied strength ratio concepts." *Can. Geotech. J.* 40 (6): 1164–1184. https://doi.org/10.1139/t03-058.

Payan, M., and R. J. Chenari. 2019. "Small strain shear modulus of anisotropically loaded sands." *Soil Dyn. Earthquake Eng.* 125 (14): 105726. https://doi.org/10.1016/j.soildyn.2019.105726.

Payan, M., A. Khoshghalb, K. Senetakis, and N. Khalili. 2016. "Effect of particle shape and validity of Gmax models for sand: A critical review and a new expression." *Comput. Geotech.* 72 (4): 28–41. https://doi.org/10.1016/j.compgeo.2015.11.003.

Petalas, A. L., Y. F. Dafalias, and A. G. Papadimitriou. 2018. "SANISAND-FN: An evolving fabric-based sand model accounting for stress principal axes rotation." *Int. J. Numer. Anal. Methods Geomech.* 43 (1): 97–123. https://doi.org/10.1002/nag.2855.

Poulos, S. J., G. Castro, and J. W. France. 1985. "Liquefaction evaluation procedure." *J. Geotech. Eng.* 111 (6): 772–792. https://doi.org/10.1061/(ASCE)0733-9410(1985)111:6(772).

Rahman, M. M., H. B. K. Nguyen, A. B. Fourie, and M. R. Kuhn. 2021. "Critical state soil mechanics for cyclic liquefaction and post liquefaction behavior: DEM study." *J. Geotech. Geoenviron. Eng.* 147 (2): 04020166. https://doi.org/10.1061/(ASCE)GT.1943-5606.0002453.

Raposo, N. 2016. "Deposição de rejeitados espessados. Caraterização experimental e modelação numérica." Ph.D. dissertation, Univ. of Porto.

Rashidian, M., K. Ishihara, T. Kokusho, M. Kanatani, and T. Okamot. 1995. "Effect of sample preparation methods on shear wave velocity." In *Proc., 2nd Int. Conf. on Seismology and Earthquake Engineering*, 1501–1508. Teheran, Iran: International Institute of Earthquake Engineering and Seismology.

Reid, D., et al. 2020. "Results of a critical state line testing round robin programme." *Géotechnique* 2020 (1): 1–15. https://doi.org/10.1680/jgeot.19.p.373.

Reid, D., and R. Fanni. 2020. "A comparison of intact and reconstituted samples of a silt tailings." *Géotechnique* 2020 (1): 1–13. https://doi.org/10.1680/jgeot.20.p.020.

Reid, D., R. Fanni, K. Koh, and I. Orea. 2018. "Characterisation of a subaqueously deposited silt iron ore tailings." *Géotech. Lett.* 8 (4): 278–283. https://doi.org/10.1680/jgele.18.00105.

Riemer, M., J. Macedo, O. Roman, and S. Paihua. 2017. "Effects of stress state on the cyclic response of mine tailings and its impact on expanding a tailings impoundment." In *Proc., 3rd Int. Conf. on Performance-based Design in Earthquake Geotechnical Engineering*. Teheran, Iran: International Institute of Earthquake Engineering and Seismology.

Robertson, P. 2021. "Evaluation of flow liquefaction and liquefied strength using the cone penetration test: An update." *Can. Geotech. J.* 59 (4): 620–624. https://doi.org/10.1139/cgj-2020-0657.

Robertson, P. K. 2010. "Evaluation of flow liquefaction and liquefied strength using the cone penetration test." *J. Geotech. Geoenviron. Eng.* 136 (6): 842–853 https://doi.org/10.1061/(ASCE)GT.1943-5606.0000286.

Robertson, P. K. 2016. "Cone penetration test (CPT)-based soil behavior type (SBT) classification system—An update." *Can. Geotech. J.* 53 (12): 1910–1927. https://doi.org/10.1139/cgj-2016-0044.

Robertson, P. K., L. De Melo, D. J. Williams, and G. W. Wilson. 2019. "Report of the expert panel on the technical causes of the failure of Feijão Dam I." Accessed April 3, 2021. http://www.b1technicalinvestigation.com/.

Robertson, P. K., and C. E. Wride. 1998. "Evaluating cyclic liquefaction potential using the cone penetration test." *Can. Geotech. J.* 35 (3): 442–459. https://doi.org/10.1139/t98-017.

Saebimoghaddam, A. 2010. "Liquefaction of early age cemented paste backfill." Ph.D. thesis, Dept. of Civil Engineering, Univ. of Toronto.

Santamarina, J. C., L. A. Torres-Cruz, and R. C. Bachus. 2019. "Why coal ash and tailings dam disasters occur." *Science* 364 (6440): 526–528. https://doi.org/10.1126/science.aax1927.

Saye, S. R., S. M. Olson, and K. W. Franke. 2021. "Common-origin approach to assess level-ground liquefaction susceptibility and triggering in CPT-compatible soils using ΔQ." *J. Geotech. Geoenviron. Eng.* 147 (7): 04021046. https://doi.org/10.1061/(ASCE)GT.1943-5606.0002515.

Schnaid, F., J. Bedin, A. J. P. Viana da Fonseca, and L. D. Costa Filho. 2013. "Stiffness and strength governing the static liquefaction of tailings." *J. Geotech. Geoenviron. Eng.* 139 (12): 2136–2144. https://doi.org/10.1061/(ASCE)GT.1943-5606.0000924.

Senetakis, K., A. Anastasiadis, and K. Pitilakis. 2012. "The small-strain shear modulus and damping ratio of quartz and volcanic sands." *Geotech. Test. J.* 35 (6): 20120073. https://doi.org/10.1520/GTJ20120073.

Shuttle, D., and M. Jefferies. 2016. "Determining silt state from CPTu." *Geotech. Res.* 3 (3): 90–118. https://doi.org/10.1680/jgere.16.00008.

Shuttle, D. A., and J. Cunning. 2007. "Liquefaction potential of silts from CPTu." *Can. Geotech. J.* 44 (1): 1–19. https://doi.org/10.1139/t06-086.

Sladen, J. A., R. D. D'Hollander, and J. Krahn. 1985. "The liquefaction of sands, a collapse surface approach." *Can. Geotech. J.* 22 (4): 564–578. https://doi.org/10.1139/t85-076.

Smith, K., R. Fanni, P. Capman, and D. Reid. 2019. "Critical state testing of tailings: Comparison between various tailings and implications for design." In *Proc., Tailings and Mine Waste*. Vancouver, BC, Canada: Univ. of British Columbia.

Soares, M., and A. Fonseca. 2016. "Factors affecting steady state locus in triaxial tests." *Geotech. Test. J.* 39 (6): 20150228. https://doi.org/10.1520/GTJ20150228.

Suazo, G., A. Fourie, J. Doherty, and A. Hasan. 2016. "Effects of confining stress, density and initial static shear stress on the cyclic shear response of fine-grained unclassified tailings." *Géotechnique* 66 (5): 401–412. https://doi.org/10.1680/jgeot.15.P.032.

Tasiopoulou, P., K. Ziotopoulou, F. Humire, A. Giannakou, J. Chacko, and T. Travasarou. 2020. "Development and implementation of semiempirical framework for modeling post liquefaction shear deformation accumulation in sands." *J. Geotech. Geoenviron. Eng.* 146 (1): 04019120. https://doi.org/10.1061/(ASCE)GT.1943-5606.0002179.

Thevanayagam, S. 2007. "Intergrain contact density indices for granular mixes—II: Liquefaction resistance." *Earthquake Eng. Eng. Vibr.* 6 (2): 135–146. https://doi.org/10.1007/s11803-007-0706-6.

Thevanayagam, S., T. Shenthan, S. Mohan, and J. Liang. 2002. "Undrained fragility of clean sands, silty sands, and sandy silts." *J. Geotech.*

Geoenviron. Eng. 128 (10): 849–859. https://doi.org/10.1061/(ASCE)1090-0241(2002)128:10(849).

Torres-Cruz, L. A. 2016. "Use of the cone penetration test to assess the liquefaction potential of tailings storage facilities." Ph.D. thesis, Faculty of Engineering and the Built Environment, Univ. of the Witwatersrand.

Torres-Cruz, L. A., and J. C. Santamarina. 2019. "The critical state line of non-plastic tailings." *Can. Geotech. J.* 2019 (1): 1–10. https://doi.org/10.1139/cgj-2019-0019.

Vaid, Y. P., J. D. Stedman, and S. Sivathayalan. 2001. "Confining stress and static shear effects in cyclic liquefaction." *Can. Geotech. J.* 38 (3): 580–591. https://doi.org/10.1139/t00-120.

Vucetic, M., and A. Mortezaie. 2015. "Cyclic secant shear modulus versus pore water pressure in sands at small cyclic strains." *Soil Dyn. Earthquake Eng.* 70 (4): 60–72. https://doi.org/10.1016/j.soildyn.2014.12.001.

Wijewickreme, D., and M. V. Sanin. 2010. "Post cyclic reconsolidation strains in low-plastic Fraser River silt due to dissipation of excess pore-water pressures." *J. Geotech. Geoenviron. Eng.* 136 (10): 1347–1357. https://doi.org/10.1061/(ASCE)GT.1943-5606.0000349.

Wijewickreme, D., M. V. Sanin, and G. R. Greenaway. 2005a. "Cyclic shear response of fine-grained mine tailings." *Can. Geotech. J.* 42 (5): 1408–1421. https://doi.org/10.1139/t05-058.

Wijewickreme, D., and A. Soysa. 2016. "Stress–strain pattern–based criterion to assess cyclic shear resistance of soil from laboratory element tests." *Can. Geotech. J.* 53 (9): 1460–1473. https://doi.org/10.1139/cgj-2015-0499.

Wijewickreme, D., A. Soysa, and P. Verma. 2019. "Response of natural fine-grained soils for seismic design practice: A collection of research findings from British Columbia, Canada." *Soil Dyn. Earthquake Eng.* 124 (4): 280–296. https://doi.org/10.1016/j.soildyn.2018.04.053.

Wijewickreme, D., S. Sriskandakumar, and P. Byrne. 2005b. "Cyclic loading response of loose air-pluviated Fraser River sand for validation of numerical models simulating centrifuge tests." *Can. Geotech. J.* 42 (2): 550–561. https://doi.org/10.1139/t04-119.

Wong, R. C., B. N. Mills, and Y. B. Liu. 2008. "Mechanistic model for one-dimensional consolidation behavior of nonsegregating oil sands tailings." *J. Geotech. Geoenviron. Eng.* 134 (2): 195–202. https://doi.org/10.1061/(ASCE)1090-0241(2008)134:2(195).

Wood, M. D., and K. Maeda. 2007. "Changing grading of soil: Effect on critical states." *Acta Geotech.* 3 (1): 3–14. https://doi.org/10.1007/s11440-007-0041-0.

Yan, W. M., and J. Dong. 2011. "Effect of particle grading on the response of an idealized granular assemblage." *Int. J. Geomech.* 11 (4): 276–285. https://doi.org/10.1061/(ASCE)GM.1943-5622.0000085.

Yang, J. 2002. "Non-uniqueness of flow liquefaction line for loose sand." *Géotechnique* 52 (10): 757–760. https://doi.org/10.1680/geot.2002.52.10.757.

Yang, J., and X. D. Luo. 2017. "The critical state friction angle of granular materials: Does it depend on grading." *Acta Geotech.* 13 (3): 535–547. https://doi.org/10.1007/s11440-017-0581-x.

Youd, T. L., and I. M. Idriss. 2001. "Liquefaction resistance of soils: Summary report from the 1996 NCEER and 1998 NCEER/NSF workshops on evaluation of liquefaction resistance of soils." *J. Geotech. Geoenviron. Eng.* 127 (4): 297–313. https://doi.org/10.1061/(asce)1090-0241(2001)127:4(297).

Zergoun, M., and Y. P. Vaid. 1994. "Effective stress response of clay to undrained cyclic loading." *Can. Geotech. J.* 31 (5): 714–727. https://doi.org/10.1139/t94-083.